

AD/A-006 101

INVESTIGATE MATERIAL SYSTEMS FOR
MIRRORS USED IN HIGH POWER CO AND CO2
LASERS

R. W. Stewart

Battelle-Pacific Northwest Laboratories

Prepared for:

Advanced Research Projects Agency
Naval Weapons Center

November 1974

DISTRIBUTED BY:

NTIS

National Technical Information Service
U. S. DEPARTMENT OF COMMERCE

AD/A - 006101

INVESTIGATE MATERIAL SYSTEMS FOR MIRRORS USED
IN HIGH POWER CO AND CO₂ LASERS

Final Technical Report

November 1974

Sponsored by Advanced Research Projects Agency

Contract #N00123-72-C-2215

ARPA Order No. 2175

Program Code No. 2D10

Contract Monitor: Naval Weapons Center
China Lake, California

Principal Investigator

R.W. Stewart
509-942-2576

Effective Date

May 22, 1972

Contract Expiration Date

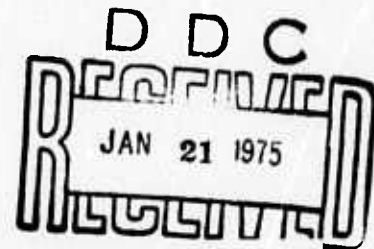
May 22, 1974

Amount of Contract

\$450,000

The views and conclusions contained in this document are those of the authors and should not be interpreted as necessarily representing the official policies, either expressed or implied, of the Defense Advanced Research Projects Agency of the US Government.

BATTELLE
PACIFIC NORTHWEST LABORATORIES
RICHLAND, WASHINGTON 99352



Reproduced by
NATIONAL TECHNICAL
INFORMATION SERVICE
US Department of Commerce
Springfield, VA. 22151

DISTRIBUTION STATEMENT A

Approved for public release;
Distribution Unlimited

INVESTIGATE MATERIAL SYSTEMS FOR MIRRORS USED
IN HIGH POWER CO AND CO₂ LASERS

by
R. W. Stewart

FINAL TECHNICAL REPORT

ABSTRACT

This report and the two preceding semiannual reports present the results of eighteen months of research aimed at demonstrating the viability of a mirror structure concept formed by sputter deposited materials. The mirror concept would be used in high energy CO, CO₂, and other infrared laser systems at the infrared wave length of 10.6 μm . Briefly, the mirror concept consisted of a support with sequential layers of a highly polishable sputtered deposit, a high reflectivity metal overlayer, and a minimum number of quarter-wavelength reflectivity enhancement coatings. Sputtered deposits of Cu-1 vol% SiC on a variety of metal substrates provided surfaces that could be reproducibly polished using conventional techniques to an rms roughness of 20 \AA or less. Although the desired reflectivity of 99.5% in the sputter deposited silver overlayer was not achieved, values of $\sim 99.2\%$ were obtained. Sputter-deposited germanium and CdTe were found to have optical properties near those of bulk material. Sputter deposition of quarter-wavelength reflectivity enhancement coatings therefore appears feasible. The results of limited laser damage testing were exceptional considering that there was not time to optimize material properties. The laser damage threshold as measured by BNW for a superpolished Cu-1 vol% SiC deposit was between 35 and 136 joules/cm²; and was 44 joules/cm² for a sputtered silver overlayer.

CONTENTS

ABSTRACT	ii
INTRODUCTION	i
TOTAL PROGRAM SUMMARY	2
Technical Problem	2
Phase I	3
Phase II	4
Phase III	4
General Methodology	5
Technical Results	5
Phase I	5
Phase II	6
Phase III	7
Department of Defense Implications	9
Implications for Further Research	10
SPUTTER DEPOSITION AND EVALUATION OF REFLECTIVITY ENHANCEMENT COATINGS	11
Experimental Procedure	11
Sputter Deposition	11
Technique for Evaluation of Optical Properties.	13
Results and Discussion	14
Germanium on NaCl Substrates	15
Physical Properties	15
Optical Properties	15

Germanium on ZnS Substrate	17
Physical Properties	17
Optical Properties	18
Germanium on Cu-1 Vol% SiC Superpolished Substrate	20
Cadmium Telluride on Germanium and NaCl Substrates	22
Physical Properties	22
Optical Properties	22
Conclusions	24
EVALUATION OF LASER DAMAGE ON SPUTTERED COATINGS	26
Experimental Procedure	26
Laser Parameters and Beam Diagnostics	26
Sample Characterization Before Testing	29
Technique for Determination of Damage Threshold	30
Results	31
Evaluation of Damage on Superpolished Cu-1 Vol% SiC Specimen	31
Evaluation of Damage on Silver Coated Specimens	33
Evaluation of Damage by Other Laboratories	34
Discussion	34
Damage Threshold on Cu-1 Vol% SiC Specimen	34
Nature of Damage on Silver Coated Specimens	36
Conclusions	36
EVALUATION OF dc SPUTTERED SILVER AS A HIGH REFLECTIVITY OVERLAYER	38
Experimental Procedure	38
Results and Discussion	39
Conclusion	42

- 1) AD-769 103
- 4) PC\$3.00/MF\$1.45
- 5) Battelle-Pacific Northwest Labs., Richland, Wash.
- 6) Investigate Material Systems for Mirrors Used in High Power CO and CO₂ Lasers.
- 9) Semiannual technical rept.,
- 10) by R. W. Stewart. (11) Aug 73, (12) 37p
- 14) BNWL-1781
- 15) Contract N00123-72-C-2215, ARPA Order-2175
- 40) Advanced Research Project Agency.

ev1/GRA 73-24 19 Nov 73

k

DO NOT PUNCH

Check List for Fields

Added Entry

	DC	SA
1	✓	
2		
4	✓	
5	✓	
6	✓	
8	-	
9	✓	
10	✓	
11	✓	
12	✓	
14	-	
15	✓	
16		
17		
18		
19		
21		
22		
23		
25		
27		
29	✓	
30		
33	✓	
34	-	
35	✓	Q

Release Date

23) Descriptors

	21	
	22	
	23	
	25	
	27	
	29	✓
	30	
	33	✓
	34	-
	35	✓/Q

25) Identifiers

27) Abstract: See reverse () Page (s) --

30) Annotated Title

29) Inventory 21

33) Dist. Code 1

34) Serial -

35) Code 401 048

FORM NTIS-59 (REV. 5-71)

DOCUMENT PROCESSING WORKSHEET

U.S. DEPARTMENT OF COMMERCE NATIONAL TECHNICAL INFORMATION SERVICE

Handwritten initials

DEPOSITION OF DISPERSION HARDENED ALLOY ON MOLYBDENUM, Cu=2 Wt% Be, AND TZM ALLOY SUBSTRATES	42
Experimental Procedure	42
Results and Discussion	42
Conclusion	43
EFFECT OF RECRYSTALLIZATION ON SURFACE FINISH	44
CONSTRUCTION AND PRELIMINARY EVALUATION OF A DIFFERENTIAL CALORIMETER FOR MICHELSON LABORATORY	44
ACKNOWLEDGMENT	45
REFERENCES	46
APPENDIX	A-1

INVESTIGATE MATERIAL SYSTEMS FOR MIRRORS USED
IN HIGH POWER CO AND CO₂ LASERS

by

R. W. Stewart

FINAL TECHNICAL REPORT

INTRODUCTION

The purpose of this report is to present and discuss results of work during Phase III of an investigation of material systems for high reflectivity infrared (IR) mirrors used in high energy CO and CO₂ lasers. Phase III is the third and final phase of an 18-month research program conducted by Battelle Northwest Laboratories (BNW) in cooperation with the Naval Weapons Center (NWC) at China Lake, California.

The overall objective of the total program was to demonstrate the feasibility of a mirror structure concept for providing the damage resistance required for use in high energy laser systems. Briefly, the mirror structure consisted of a support with sequential layers of a (1) highly polishable sputtered deposit, (2) a high reflectivity metal overlayer, and (3) a minimum number of quarter-wavelength ($\lambda/4$) reflectivity enhancement coatings. Details of the mirror structure have been presented previously. (1, 2)

The Phase I work dealt with development of the highly polishable ($<15 \text{ \AA rms}$) sputtered deposit; and metallurgical characterization,

polishing, surface roughness and optical absorption techniques.⁽¹⁾ In Phase II, the development concentrated on the high reflectivity metal overlayer, although problems with reproducibility of sputtered deposit properties and polishing techniques required a larger than anticipated amount of attention for resolution.⁽²⁾ The Phase III work centered on development of reflectivity enhancement coatings and evaluation of laser damage on Cu-1 vol% SiC and silver, with some effort devoted to completion of work on providing dispersion hardened coatings for evaluation, determination of the influence of recrystallization on surface finish and evaluation of silver overlayers deposited by dc sputtering.

TOTAL PROGRAM SUMMARY

TECHNICAL PROBLEM

The ultimate objective of the program was to establish optimum material parameters for obtaining high performance mirrors for use in high energy lasers. Specifically this goal was to be met by employing sputter deposited materials for the various elements of a mirror structure concept consisting of the following components:

- 1) A metal mirror support upon which the sequence of layers indicated in 2, 3 and 4 below are formed.
- 2) A hard, stable, fine-grained, sputter-deposited (≈ 0.25 mm thick) material, whose principal property is its ability to be mechanically polished to a surface roughness of $\leq 20 \text{ \AA}$ rms.
- 3) A thin sputter-deposited high conductivity metal overlayer for improving mirror reflectivity.

- 4) A two-component $\lambda/4$ reflectivity enhancement coating sputter-deposited on the metal overlayer for further improvement of mirror reflectivity.

The program was divided into three phases--work in Phase I emphasized the polishable material, Phase II emphasized the metal overlayer, and Phase III emphasized the reflectivity enhancement coating and laser damage evaluation. The specific objectives for the three phases as presented in the contract, are given below. Comment is provided in the Technical Results section concerning the modification in the objectives found to be necessary during the performance of the work.

Phase I

Objectives, in order of priority:

- 1) Investigation of sputtering metal onto metal substrate and subsequent polishing which results in either (a) a surface exhibiting an rms surface height of 20 \AA , or (b) definition of procedures necessary to attain that smoothness. Initial substrate selection - OFHC copper and at least one other candidate material.
- 2) Sufficient characterization of the prepared samples to allow identification of those approaches most likely to result in further improvements.
- 3) Development of supporting instrumentation,
 - (a) Calorimeter for mirror absorptance measurements with 10% accuracy operational,

- (b) Scattered light measuring instrument operational,
 - (c) Study of feasibility of optical heterodyne technique for roughness evaluation started.
4. Initiation of investigation of low pressure sputtering for high reflectance metal overlayer.

Phase II

Objectives, in order of priority:

- 1) Reach a decision as to whether a sputtered metallic overlayer can be achieved which exhibits an absorption of less than 0.005 at 10.6 μ and, if not, achieve such an absorption by vacuum deposition.
- 2) Electrical and metallurgical characterization of the high reflectance overlayers and correlation with optical properties.
- 3) Initiate deposition of reflectance enhancing dielectric coatings.
- 4) Laser damage studies initiated.
- 5) Evaluation and, if possible, laboratory demonstration of the optical heterodyne technique complete.

Phase III

Objectives, in order of priority:

- 1) Dielectric enhancement coating identified and satisfactory depositions made.
- 2) Curved mirror with 1.43 meter radius of curvature, 1.52 inch diameter exhibiting absorption of less than 0.001 at selected wavelengths between 2 μ and 10.6 μ fabricated.

- 3) Data for extent of and threshold for damage in developed mirrors obtained.

In addition to the above goals, a general goal will be to try the techniques (sputtering, polishing, overcoating, etc.) developed herein on as many candidate substrate materials as the program schedule allows.

GENERAL METHODOLOGY

The approach utilizes laboratory scale sputtering technology for the development of a mirror structure with subsequent characterization and evaluation of the structures formed with respect to metallurgical and optical properties.

TECHNICAL RESULTS

Phase I

As summarized below objectives 1, 2 and 3 were successfully accomplished. Time and funds did not permit initiation of activity on objective 4.

The original concept that dispersion hardened sputter deposited material would exhibit improved polishability was demonstrated. A surface roughness of $\approx 15 \text{ \AA}$ rms was consistently obtained by mechanically polishing sputtered 0.3 mm thick deposits of copper, dispersion hardened with 1 vol% SiC. This marked the first time that a surface roughness $\leq 20 \text{ \AA}$ rms had been obtained by mechanically polishing a metal surface. The material properties of principal importance contributing to this result were found, in order of importance, to be a small and stable grain size $\leq 0.4 \text{ \mu m}$, material homogeneity, with some contribution from increased hardness. In addition, a sufficient amount of

dispersoid (SiC) must be introduced into the copper to ensure microstructural stability in the temperature range where the mirrors are expected to operate. Recrystallization which may occur at prolonged operation at elevated temperatures results in increased surface roughness and reduced reflectivity. The principal deposition parameters for reproducibly achieving the required material properties were established.

Apparatus for absorption and surface roughness measurements was developed and satisfactorily placed into use.^(1,2) A theoretical analysis was performed which indicated that use of an optical heterodyne technique for surface roughness measurement was feasible. In addition, the application of Nomarski Differential Interference Contrast Microscopy was found to be very useful for qualitative surface roughness evaluation. The bowl-feed polishing technique for quartz initially prescribed by Michelson Laboratory was found to be unsuitable for polishing the Cu-1 vol% SiC sputtered deposit. Therefore, the development of a bowl-feed polishing procedure based on a cloth lap and a colloidal carbon slurry by BNW was considered essential to the successful completion of Phase I. In subsequent work at Michelson and other laboratories it was found that adjustment of the pH of the polishing slurry resulted in the ability to obtain the desired surface roughness and mirror figure with conventional bowl-feed techniques.

Phase II

As summarized below, objectives 1 and 2 were only partially accomplished. Within the time and funds provided it was not possible to initiate work on objectives 3 and 4. Objective 5 was eliminated from the program through mutual agreement with Michelson Laboratories at the Naval Weapons Center, China Lake, California.

Thin ($\approx 1500 \text{ \AA}$) sputter-deposited pure copper and silver high conductivity Cu-1 vol% SiC overlayers were deposited on smooth

(<20 Å rms) polished, dispersion hardened, Cu-1 vol% SiC substrates to reduce IR absorption in the surface. Maximum reflectivity of 99.12 and 99.2% and minimum absorption of 0.88% and 0.83% were obtained for copper and silver, respectively. This absorption is 0.2-0.3% higher than expected based on total reflectivity measurements on UHV evaporated copper and silver films. Both rf-diode and dc-supported plasma sputtering techniques produced essentially the same properties in the overlayer deposits. The principal deposition parameters important to maintaining low surface roughness and obtaining high reflectivity in the overlayer were deposition rate and substrate temperature. The goal of obtaining a reflectivity of 99.5% was not met.

Although outside of the scope of the original program, dispersion hardened sputtered deposits of Cu-1 vol% SiC on OFHC copper were provided to three independent laboratories, at the request of Michelson Laboratories. All demonstrated that the sputtered deposit could be polished to ≤ 20 Å rms surface roughness with one laboratory reproducibly obtaining ≈ 15 Å rms.

Phase III

As summarized below, objectives 1 and 3 were successfully accomplished. Objective 2 had been eliminated during discussions with M. J. Stickley, DARPA, which took place during the Phase I period of the contract.

The results of the initial experiments on sputter deposition of candidate materials for $\lambda/4$ reflectivity enhancement coatings were encouraging. Sputtered deposits of both germanium and CdTe had properties close to those of bulk material. The values obtained for refractive

index of germanium and CdTe, and absorption index of germanium plus density, composition and structure data indicate that the use of such materials for $\lambda/4$ stack reflectivity enhancement coatings is feasible.

Threshold values for laser damage were established on two mirror surfaces. On one, a superpolished dispersion hardened Cu-1 vol% SiC alloy surface, two different values were obtained which depend on the method used to analyze damage. One value, determined from the maximum diameter of the damage area and the laser beam energy density resulting from a full beam exposure at that diameter, was 136 joule/cm². The other, determined by extrapolation of the relationship between damage area diameter and attenuated laser beam energy density resulted in a value of 35 joule/cm². It is pertinent to note that the 136 joule/cm² threshold is $\sim 300\%$ higher than previously observed on polished metal surfaces.

The second mirror surface subjected to laser damage evaluation was a superpolished dispersion hardened Cu-1 vol% SiC alloy surface with an $\approx 1500 \text{ \AA}$ sputter-deposited silver overlayer. Using the extrapolation damage analysis method above, a damage threshold of 44 joule/cm² was obtained.

The development of reflectivity enhancement coatings did not reach the point where laser damage studies could be initiated.

Deposition of silver reflectivity enhancement overlayers by dc sputtering was found to result in essentially the same reflectivity as obtained by rf sputtering.

In discussions with Michelson Laboratories it was agreed that although outside of the scope of the original program, the work summarized in the following was necessary. A duplicate of the differential calorimeter developed by BNW for mirror absorption measurements was assembled, tested and provided to Michelson Laboratories to augment their optical characterization capability. Recrystallization of a Cu-1 vol% SiC deposit at 450°C was found to increase the surface roughness from 19 Å to 50 Å rms. Deposits of Cu-1 vol% SiC were made on polished molybdenum, Cu~2 wt% Be and TZM alloy substrates for evaluation by Michelson Laboratories and BNW. The different substrates did not have any measurable effect on deposit polishability and the 16 Å rms surface roughness obtained by Michelson Laboratories was essentially identical to the 13-16 Å rms range obtained by BNW.

DEPARTMENT OF DEFENSE IMPLICATIONS

The results of the program indicate that BNW high rate sputtering technology could be beneficially used in the fabrication of high performance mirrors for use with high energy lasers. Without opportunity for optimization, the materials developed proved to be highly polishable with resistance to laser damage beyond that known to be available from other methods of fabrication. It is the opinion of BNW that additional work on the utilization of sputtering technology for mirror fabrication be initiated.

IMPLICATION FOR FURTHER RESEARCH

The work in this contract was aimed at establishing feasibility for utilization of high rate sputtering technology in several areas of research and to that end was successful. Future work on application of high rate sputtering should proceed in two parallel paths. One path would consist of mirror fabrication for test and evaluation, based on the existing state-of-the-art. The other would pursue research on mirror materials and optimization of their properties for use in mirror fabrication.

SPUTTER DEPOSITION AND EVALUATION OF REFLECTIVITY
ENHANCEMENT COATINGS

The objective of this research was to determine if candidate dielectric and/or semiconductor materials for $\lambda/4$ reflectivity enhancement coatings (REC) can be deposited by sputtering to obtain the required optical properties at 10.6 μm wavelength.

EXPERIMENTAL PROCEDURE

Sputter Deposition

Both Ge and CdTe materials were deposited in a modified conventional diode radio-frequency (rf) sputtering system. It consisted of an 18-in. stainless steel water-cooled bell jar sealed to the base plate and top plate with Viton-L gaskets. The bell jar was pumped with a standard 2400 μsec oil diffusion pump combined with 140 μmin mechanical pump, and trapped with a high conductivity, high efficiency liquid nitrogen trap.

The electrode arrangement is illustrated in Figure 1. The sputtering target was located in the center of the lower baseplate. The substrate was located directly above and supported from the top plate. The distance between the two electrodes could be varied from 3/4 in. to 4 in. A removable shutter could be introduced at any selected position in the space between the electrodes. Most frequently, when in the closed position, the shutter was approximately 1/8 in. from the substrate surface. In most cases the target-substrate distance was 1.25 in.

For Ge the deposition rate was varied by changing the rf forward power between 100 and 500 watts, corresponding to a target power density of ≈ 1.6 watts/cm² and 8 watts/cm², respectively. The relation between deposition rate and power density is presented in Figure 2. The substrate temperature was varied from 3°C to 400°C. It was measured by a thermocouple located in the substrate holder adjacent to the substrate. The wedge-type clamping arrangement of the substrate in its holder ensured good heat transfer between the two. Since it was clamped at the circumference, however, temperature gradients in the substrate were assumed to be present, at least in the case of NaCl and ZnS substrates.

Use of several variations in deposition parameters were attempted for deposition of CdTe on germanium, NaCl, SiO₂, and OFHC copper substrates. All deposits however, made at power densities above 3.2 watts/cm² had increased surface roughness and partially peeled from the substrate.

The germanium and CdTe sputtering targets were obtained from Haselden, Inc., San Jose, California. The material purity as quoted by the vendor was 99.99% for germanium, and 99.999% for CdTe. These targets were placed in a copper dish at elevated temperature ($\approx 100^\circ\text{C}$) to permit shrink fitting for firm holding in the dish upon cooling. Subsequently the target assembly was bolted to a water-cooled staging platform associated with the rf feedthrough electrode. This system for target attachment was used rather than an eutectic bonding procedure to minimize possible target contamination. Although cracks formed in the targets during use, they were not large enough to cause contamination from the copper backing.

The sputtering gas was AIRCO Argon Special Order Grade 4-1M certified 99.999% pure. The system gas pressure (normally $\approx 1 \times 10^{-2}$ torr) was maintained with a Granville-Phillip's pressure controller, coupled with a Schultz-Phelps' ionization vacuum gauge. The pressure and gas flow in the bell jar were regulated by a controller-operated needle inlet valve and a pump throttling valve. The latter was located at the pumpout port in the baseplate. The gas flow rate through this valve was selected by installing a suitable orifice in the valve plate. During system pumpdown, or whenever maximum conductance was required, the valve was removed. Typical deposition conditions for both germanium and CdTe were as follows:

Target Substrate Spacing	1.25 inches
Argon Gas Pressure	1×10^{-2} torr
Target Power (13.56 MHz)	3.23 watt/cm ²
Substrate Temperature	5-300°C
Substrate Potential	dc-Floating, rf-Grounded
Deposition Rate	0.125 $\mu\text{m}/\text{min}$ germanium, 0.7 $\mu\text{m}/\text{min}$ CdTe

Technique for Evaluation of Optical Properties

The optical properties of a material are determined by its complex index of refraction, $\hat{n} = n + ik$, where n is the refractive index and k the absorption index. Determination of the refractive index requires deposition of the candidate material, i.e., germanium or CdTe, on transparent substrates with significantly different indices in the wavelength range of interest. Transmission spectrophotometry can then be used to determine the optical thickness of the deposit. An independent

measurement of physical thickness permits determination of the refractive index. Briefly, the procedure for determination of optical properties is given in the following:

- Transmission spectrophotometric observations are first performed on a relatively thick deposit $h \approx 20 \mu\text{m}$, to determine optical thickness. The optical thickness is then derived using the physical thickness estimated from deposit weight and area. This information permits determination of the sputtering run duration necessary to deposit $\lambda/2$ thickness layers on the transparent substrate.
- Material absorption is determined by depositing a $\lambda/2$ thick layer on a super-smooth metal substrate whose absorption has previously been determined. The actual optical thickness of the layer is then determined by reflection spectrophotometry. This sample is next subjected to a calorimetric absorption measurement. The absorption index of the deposit is determined by comparing the observed absorption increase to that calculated with a computer program, using the absorption index, k , as the independent parameter.

A brief outline of the theoretical background and details of the absorption measurement technique and calculations are presented in Appendix A.

RESULTS AND DISCUSSION

Substrates of both NaCl and ZnS were used in the investigation of the optical properties of sputtered germanium. The results are discussed separately below.

Germanium on NaCl Substrates

Physical Properties

Germanium deposited on NaCl at substrate temperatures in excess of 150°C had increased surface roughness, a foggy appearance, and frequently separated from their substrates either during deposition or upon removal from the sputtering system. As determined by x-ray diffraction, at lower substrate temperatures (i.e., 5°C) the germanium deposits were amorphous while at a substrate temperature of 300°C they were polycrystalline with a pronounced fiber structure. The growth direction in the fiber texture was $\langle 100 \rangle$ perpendicular to the substrate, and the grain size was approximately 0.1 μm . The exact transition temperature from amorphous to polycrystalline was not determined, but it is of interest to note that the 300°C temperature where we observed polycrystalline structure was lower than the 330°C reported by Krekorian.⁽³⁾ It should also be noted that since our deposition rate was about 10 times higher than Krekorian's our crystallization temperature should be higher than 330°C. No explanation can be offered for this observation.

Optical Properties

Sputtering conditions and spectrophotometer data showing results obtained with NaCl substrates are listed in Table 1. Values for optical thickness were obtained by measuring the wavelength separation between maxima and minima on the spectrophotometer trace. Entries in Table 1 for refractive index were obtained by self-consistent analysis of the magnitudes of the transmission at quarter-wave points (near 10.6 μm wavelength) as presented in Appendix A. For this series of measurements

the spectrophotometer was improperly balanced. Consequently, the entries for n and h are to be considered as estimates only. Estimated values for the refractive index, n , are within 1.5% of the 4.0 value for bulk germanium.

Table 1. Sputtering Conditions and Spectrophotometer Results for Germanium Deposited on NaCl

<u>Deposit</u>	<u>Deposition Duration (sec)</u>	<u>Substrate Temperature (°C)</u>	<u>Optical Thickness nh (μm)</u>	<u>Refractive Index-n</u>	<u>Derived⁽¹⁾ Thickness-h (μm)</u>
5	7200	Cold	23.62	4.058	5.82
6	3600	10	20.55	4.058	5.06
7	3600	47	22.58	4.006	5.56
9	60	155	-	-	~.155
10	120	146	.842	4.22	.209
11	180	162	1.359	4.031	.337
14	3600	42-56	27.199	4.035	6.741

(1) Derived from optical thickness and refractive index

The slope of the absorption edge is generally considered an indicator of the purity of the sample, pure germanium exhibiting a sharp edge. A comparison of the absorption edge of Ge-NaCl #5 and bulk polycrystalline germanium is given in Figure 3, which shows the external transmittance in the wavelength range $1.3 \mu\text{m} \leq \lambda \leq 2.6 \mu\text{m}$. The transmittance of the deposit changes more slowly with wavelength than that of bulk germanium. Significant transmission of the deposit can be detected at $\lambda = 1.7 \mu\text{m}$, where sinusoidal dependence of transmittance on wavelength, characteristic of

interference effects, is evident. In the trace for bulk germanium, discernible rise above zero transmittance does not occur until about $\lambda = 1.76 \mu\text{m}$.

An estimate of the dependence of refractive index and absorption (i.e., dispersion) for the deposit, Ge-NaCl #5 can be made from the data shown in Figure 3. Theory predicts that the deposit-substrate combination should possess the transmission of the substrate at half-wave points, i.e., maxima in the trace for Ge-NaCl #5 shown in Figure 3, while the distance between maxima and minima is determined by the optical thickness of the layer. This analysis indicates that the refractive index changes from approximately $n = 4.21$ at $\lambda = 1.7 \mu\text{m}$ to $n = 4.058$ at $\lambda = 2.5 \mu\text{m}$. Over the same wavelength range, comparison of observed transmittance of the combination to that calculated for NaCl indicates that the absorption of the deposit decreases from approximately 0.9 to 0.6. This decrease is probably due to free carrier absorption. Whether the additional free carriers are due to structural defects or impurities is not known at this time. Difficulty with unpredictable flaking of germanium deposited on NaCl substrates prompted a change to ZnS substrates. Experience with these deposits is given in the following section.

Germanium on ZnS Substrate

Physical Properties

The physical properties of germanium sputter deposited on ZnS substrates were substantially the same as those observed for acceptable deposits on NaCl substrates. Problems with lack of deposit adherence and variability of deposit character over the surface of the substrate

were not encountered with ZnS substrates. Experience gained indicates that ZnS is a much more suitable substrate for sputter deposition of germanium than is NaCl.

Optical Properties

Results of optical characterization of germanium deposits on ZnS substrates are given in Table 2. No index values were obtained for deposits I and II because of improper balance on the spectrophotometer.

Table 2. Data Obtained from Germanium Deposited on ZnS Substrates

<u>Deposit</u> ⁽¹⁾	<u>Optical Thickness</u> <u>nh (μm)</u>	<u>Refractive Index-n</u>	<u>Derived</u> ⁽²⁾ <u>Thickness-h</u> <u>(μm)</u>	<u>Physical</u> ⁽³⁾ <u>Thickness</u> <u>(μm)</u>	<u>SEM</u> ⁽⁴⁾ <u>Thickness</u>
I	26.76	-	6.68 ⁽⁵⁾	6.23	5.5
II	21.19	-	5.29 ⁽⁵⁾	5.36	4.25
III	23.22	4.006 ⁽²⁾	5.80	5.3	-
IV	4.703	4.106 ⁽²⁾	1.14	-	-
V	2.349	4.047 ⁽²⁾	.58	-	-

(1) Deposited at substrate temperature below 200°C

(2) Derived from optical thickness and refractive index

(3) Measured from mass and dimension of deposit

(4) Determined by scanning electron microscope (SEM)

(5) Determined using the refractive index of deposit III

It is of interest to note that the thickness derived from self-consistent analysis of spectral data agrees with that estimated from deposit mass and area to within 10%. The germanium deposits of Table 2 therefore possess index and density close to bulk germanium.

A representative spectrophotometer trace of deposit Ge-ZnS #III (Table 2) is presented in Figure 4. External transmittance of a ZnS substrate is also presented. It is to be emphasized that the self-consistent analysis described in Appendix A and used to derive numbers in Table 2 does not include the absorption index k . Theory predicts that for films with half-wave thickness, i.e., $nh = m \lambda/2$, and with $k = 0$, the optical properties at any wavelength λ of the deposit/substrate combination are only those of the substrate. At half-wave points a zero absorption deposit layer should have the same optical properties as the substrate. Accordingly, in the trace for Ge-ZnS #III shown in Figure 4, if the film has $k = 0$, the transmission maxima of the deposit-substrate combination should coincide with the external transmittance of the substrate. Some loss due to the deposit is evident in the trace. Consequently, index values derived from the trace of Figure 4 are not accurate. The loss is low, however, because the trace for the deposit-substrate combination gets very close to that for the uncoated substrate at transmission maxima.

Deposits IV and V of Table 2 were made as a final step in preparation for deposition of a half-wave thickness ($\frac{\lambda}{2}$) layer on a metallic substrate for film absorption determination. The object of these deposits was to obtain $\lambda/2$ and $\lambda/4$ layers to minimize the effects of absorption on index determination and to obtain deposition rate data pertinent to the deposition of a $\lambda/2$ layer on metal. Spectral data for these deposits are shown in Figure 5. Optical thickness of the deposits as determined from the data in Figure 5 are actually slightly less than desired, but the ratio $nh(\text{IV})/nh(\text{V}) = 2.002$ is within 0.1% of the factor

of 2 required. Since duration of the sputtering run was the only difference between deposits IV and V, this serves as evidence that deposits of desired thickness can be obtained by accurate control of deposition conditions and duration of deposition. The average of indices obtained from spectral data for deposits IV and V was $n = 4.07$. That value was used in calculations for determination of absorption index k by comparison to absorption measurements.

Germanium on Cu-1 Vol% SiC Superpolished Substrate

Reflection spectrophotometric data for a half-wave thick germanium layer deposited on Cu-1 vol% SiC superpolished ($\sim 17 \text{ \AA}$ rms) BNW mirror substrate 044#30 are shown in Figure 6. Using the wavelength difference between maxima and minima, the optical thickness of the deposit was determined to be $nh = 5.383 \text{ \mu m}$, within 1.6% of $\lambda/2$ at 10.6 \mu m . Low but finite absorption is evident since the trace for the combination does not touch that for the substrate at reflection maxima. Plots of reflected energy versus absorbed energy for both the metal surface and the half-wave germanium layer deposited on that sample are shown in Figure 7. The absorption is derived from the slope of the curves, as discussed in Appendix A. The $\lambda/2$ thick germanium layer was found to increase absorption by 3.95×10^{-3} . The complex index of the metal substrate surface was determined to be $(n_2, k_2) = (24.83, 76.42)$ using arguments presented in Appendix A and the absorption of the metal as derived in Figure 7. Using the complex index of the substrate; the absorption of the deposit/substrate combination; deposit thickness and refractive index; and the method discussed in Appendix A; the relationship between absorption index of the deposit and the calculated

absorption of the deposit/substrate combination illustrated in Figure 8 was obtained. Determination of the absorption index of the deposit is accomplished through the relationship in Figure 8 by simply finding that value which predicts the observed absorption, Figure 7. The values obtained from the above analysis are presented in Table 3.

Table 3. Optical Constants of $\lambda/2$ Ge-Cu-1 Vol% SiC Combination

<u>Material</u>	<u>Surface Roughness, Å, rms</u>	<u>Absorption (%)</u>	<u>(n,k)</u>
Substrate	14	$1.526 \pm .045$	(24.83, 76.42)
Combination	27	$1.921 \pm .036$	-
$\lambda/2$ Germanium Layer	-	$.395 \pm .087$	[4.07, $(5.12 \pm 1.1) \times 10^{-3}$]

The significance of these data is discussed in the following. The germanium deposit exhibits an intensity absorption coefficient ($\frac{4\pi k}{\lambda}$) of about 60 cm^{-1} . This may be compared with the value obtained by Spicer and Donovan⁽⁴⁾ who quote an upper limit of 10 cm^{-1} for the absorption coefficient in evaporated amorphous germanium deposits for wavelengths greater than about $2.5 \mu\text{m}$. More recent results on germanium deposits made by physical vapor deposition indicate an absorption coefficient of about 40 cm^{-1} at $10.6 \mu\text{m}$.⁽⁵⁾ Thus the absorption coefficient in sputtered germanium appears to be higher than that reported by other investigators.

The reasons for the larger absorption coefficient exhibited in sputtered germanium may lie partly in the fact that the deposition

conditions were not optimum for obtaining minimum absorption, and partly due to uncertainty as to the purity of the sputtering target. Other workers⁽⁵⁾ have demonstrated that the purity of the starting material is important to obtaining a low absorption coefficient.

Cadmium Telluride on Germanium and NaCl Substrates

Cadmium telluride deposits were made on NaCl, germanium, SiO₂, and OFHC polished copper substrates, all at low substrate temperatures (<10°C). Analytical results obtained from selected deposits are presented below.

Physical Properties

The CdTe deposits were all polycrystalline exhibiting a fiber structure, even at a substrate holder temperature of 3°C. Based on x-ray diffraction the structure was cubic containing a large number of stacking faults probably due to the influence of deposition conditions on growth. The growth direction of the cubic structure was mainly <111> perpendicular to the substrate. There was no evidence of any other phase than CdTe. The crystallite size appears to be in the range from 0.1 μm to 1 μm. Uncompensated electron probe measurements of composition indicate a Te-Cd weight percent ratio of 1.135 compared to a theoretical ratio of 1.13. The deposit is therefore nearly the stoichiometry of CdTe.

Optical Properties

Work with CdTe proceeded to the point where satisfactory deposition conditions were established, and thick deposits for spectrophotometric analysis were made on both germanium and NaCl substrates. Data obtained from the deposits is presented in Table 4. External transmittance data

Table 4. Data on CdTe Deposits⁽¹⁾

Substrate	Optical Thickness nh (μm)	Optical ⁽²⁾ Refractive Index-n	Derived ⁽²⁾ Thickness h (μm)	Physical ⁽³⁾ Thickness (μm)	Refractive ⁽⁴⁾ Index
Germanium	57.06	2.69	21.21	21.0	2.65
Germanium	13.26	2.63	5.05	4.9	2.71
NaCl	61.77	2.56	24.13	20.8	2.97

(1) Deposited at substrate temperatures of 305°C at a power density of 3.2 watts/cm².

(2) Derived from optical thickness and spectral data.

(3) Measured from mass and dimensions of deposit.

(4) Derived from optical and physical thickness values.

for two of the CdTe deposits on germanium substrates are compared to that of a germanium substrate in Figure 9. The transmittance enhancement behavior expected from deposition of a low index layer on a high index substrate, is evident, even for the very thick layer. A qualitative estimate of "low" for the absorption of these deposits can be projected on the basis of the degree to which the transmittance for the coated samples approach that of the germanium reference sample at half-wave points. The trace for the 9 μm thick deposit layer actually touches that for the substrate at $\lambda = 6.56 \mu\text{m}$ and is extremely close to it at $\lambda = 8.85 \mu\text{m}$ and $\lambda = 13.5 \mu\text{m}$. At these points the transmissivity of the sample is within 0.64% of the theoretical transmissivity of the substrate. Although quantitative absorption measurements were not made from these data a low absorption deposit is indicated.

External transmittance for a thick CdTe layer on a NaCl substrate is presented in Figure 10. Physical thickness is estimated to be 20.8 μm on the basis of mass increase and deposit area, while transmittance data yield a thickness of 24.13 μm . The value derived from transmittance data is undoubtedly more accurate, since the refractive index obtained from the mass-area estimate predicts a transmittance at quarter-wave points of 48.9%, far from the value of 59.0% actually observed. This result is not surprising, but is also not completely understood. The simplest explanation of the discrepancy postulates that the NaCl substrate may have lost mass prior to and during deposition.

Detailed results of analysis of spectral data for Figures 9 and 10 are given in Table 4. Agreement between optical and physical estimates of index and physical thickness for the deposits on germanium substrates is strong evidence that the deposits possess density and index near that of bulk CdTe.

Towards the end of the program, conditions for satisfactory deposition of CdTe on OFHC copper were established. The samples were prepared for the purpose of qualitative measurement of absorption. Reflection spectral data was, however, not obtained, but the deposits exhibited excellent mirror appearance under optical microscope evaluation.

CONCLUSIONS

Although considerable additional work on characterization of the deposits and improved definition of optimum deposition conditions

are required, the results indicate that deposition of optical quality materials by high rate sputtering is indeed possible. The approach may prove to have significant advantages in preparation of optical films for applications in the IR regime.

EVALUATION OF LASER DAMAGE ON SPUTTERED COATINGS

In this part of the program, work was directed toward determination of the extent of, and threshold for, laser damage at $\lambda = 10.6 \mu\text{m}$ on polished samples of sputter-deposited Cu-1 vol% SiC, with and without a sputtered silver overlayer. Experiments on two BNW mirror samples were conducted in the Energy Beam Physics Laboratory at Battelle-Columbus (BCL).

EXPERIMENTAL PROCEDURE

Laser Parameters and Beam Diagnostics

The arrangement of the optical components, the vacuum system and the sample position in the laser damage experiments, are presented in Figure 11. A Lumonics TEA-CO₂ laser with 60 joule multimode output was used. The laser was forced to oscillate in the TEM₀₀ mode by inserting an aperture of one cm diameter inside the cavity near the germanium output mirror. Energy output in the TEM₀₀ mode was 0.55 joule. In the cavity, the rear mirror had a radius of 21 m, the front mirror was flat and the distance between them was 1 m. Total beam energy was measured by a Hadron Model 107 cone calorimeter. A Rolfin Ltd. photon drag detector was used to determine the time history of the laser pulse. A pair of folding mirrors near the laser directed the beam to the sample chamber, approximately 9 m from the laser source. A system of 3 flat mirrors, two of which were external to the target chamber, was used to bring the beam to the focusing mirror, $f = 20 \text{ cm}$. Samples were mounted on a movable stage such that the sample surface was in the focal plane of the 20 cm mirror. Total beam energy was observed external to the

target chamber, just in front of the 3-mirror system. The photon drag detector was mounted inside the chamber and could be arranged to detect either the unfocused beam or the beam reflected from the target.

Operation in the TEM_{00} mode was extremely sensitive to laser cavity alignment. Cavity alignment was repeatedly checked by observing the burn pattern produced on Thermofax paper by the unfocused beam at a position of 1.5 m from the laser, and by monitoring the total energy output on the calorimeter. Total output was found to be a sensitive indicator of fundamental mode operation; maximum output of 0.55 joule consistently corresponded to a round spot on the Thermofax paper. Slight misalignment resulted in detectable lobes in the burn pattern and a decrease in beam energy. Energy delivered to the target was 0.52 joule, reduced from the 0.55 joule value by 6% due to the input mirrors and the salt window on the vacuum chamber. Controlled attenuation of the beam to values below 0.55 joule was achieved by the use of 12 different combinations of attenuators. Detailed distribution of energy in the focal spot was determined by observing the focal spot radius produced on cellulose acetate as a function of beam attenuation. In addition to the full beam exposure, attenuators with transmission between 0.66 and 0.012 were used. Therefore average incident energies ($T_i E$) of $0.55 \text{ j} > T_i E > 0.0066 \text{ j}$ were available for determining beam profile. Calibration of the attenuators was verified by both calorimetric observations and comparison of photon drag detector signals.

Peak energy density in the focal spot is W_0 with the unattenuated beam, $T = 1$. Since cellulose acetate possess a definite threshold value, there exists some critical transmission, T_c for which no effect on the

material will be observed for an incident maximum energy density of $T_c W_0$. For a Gaussian beam, the radius r_i produced on the material when the beam passes through an attenuator with transmission T_i is related to T_c and the 1/e radius of the intensity distribution, a , by

$$\frac{T_c}{T_i} = e^{-(r_i/a)^2} \quad (1)$$

A least-squares fit of a Gaussian curve to a plot of (T_c/T_i) versus r_i thus allows determination of both T_c and a . Calorimetric measurement of total beam energy E_c then allows definition of both the beam profile and threshold for the material. Results, illustrated in Figure 12 show that the beam profile is given by

$$W(r) = W_0 e^{-(r/a)^2}, \text{ where} \quad (2)$$

$$W_0 = E_c/\pi a^2 = 251 \pm 21 \text{ joule/cm}^2,$$

$$a = 0.0256 \pm 0.001 \text{ cm},$$

$$T_c = 0.0143.$$

Since the 1/e radius of a Gaussian beam from a 1-cm aperture focused by a mirror of 20-cm focal length is 0.0259 cm, the value 0.0256 ± 0.001 cm for "a" verifies fundamental mode operation. The uncertainty of 8.6% in W_0 was estimated from the statistics of the least square fit.

Typical time dependence of output power in the TEM_{00} mode is presented in the photon drag detector record in Figure 13. Partial mode-locking is evident in the rapid oscillations (Figure 13-b). Due to these modulations in the beam instantaneous peak power density in the focal spot could therefore be significantly higher than the average

power. The equivalent pulse, i.e., the square pulse at peak amplitude which encloses area equivalent to that of the actual pulse, has a duration of 470 nsec. Equivalent average power density in the focal spot is thus 5.3×10^8 watts/cm².

Sample Characterization Before Testing

To permit determination of the effects of surface roughness on laser damage threshold in these materials each sample was subjected to extensive characterization prior to damage experiments. Optical absorption at 10.6 μm was determined using the BNW calorimeter.⁽¹⁾ Scattering measurements of surface roughness were obtained at four positions each along two diameters of the sample, separated by 90°. Nomarski photomicrographs of surface topography were obtained in regions near those where scattering measurements had been made. A total of four samples were subjected to this extensive characterization. Because of a time limitation, only two samples were used in the damage experiments.

To determine if improvement in damage resistance could be realized with a sputter deposited silver overlayer, a comparison between the superpolished Cu-1 vol% SiC alloy and a sputtered silver surface was obtained. The sputtered Cu-1 vol% SiC alloy was deposited on superpolished Cu-2 wt% Be mirror support, BNW 045 #39. The silver overlayer was sputter deposited on Cu-1 vol% SiC using techniques previously described in this report. The sputter deposition of Ag on sample #012 changed the surface only slightly resulting in about 2 Å rms increase in surface roughness from that of the original surface. Typical

pre-test characterization data for the samples used in these experiments are given in Table 7.

Table 7. Results of Pretest Characterization of Samples for Laser Damage Experiments*

<u>Sample</u>	<u>Material</u>	<u>10.6 μm Absorption %</u>	<u>Distance from Edge, cm</u>	<u>Surface Roughness \AA rms</u>
045 #39	Cu-1 vol% SiC on Cu-2 wt% Be Substrate	1.74	3.15**	13.7
			2.64	15.1
			2.14	17.5
			1.63**	15.4
0 12	Ag Overlayer on Cu-1 vol% SiC Support	1.1	3.06	19.0
			2.55**	21.0
			2.04	21.0
			1.54	20.0

* Data obtained from one major diameter on each specimen.

** Laser damage exposures near these positions.

Technique for Determination of Damage Threshold

Original plans called for determination of damage threshold by in situ observation of a micro-discharge at the position of exposure, a technique suggested by others. (6) To avoid contamination of the mirror surface, a low pressure liquid nitrogen-trapped system was used. The pressure in the system during damage experiments was maintained between 2×10^{-6} and 5×10^{-5} torr. This, however, was apparently too low to permit formation of a visible plasma. Observation of the exposed region with a 10X telescope revealed visible flashes only occasionally at maximum intensity. Since no reliable in situ means of estimating

damage threshold was available, it was decided to use postexposure analysis for determining threshold.

Two methods for determining threshold values by examination of exposed regions were established. One method relies on relating the damage area produced by the unattenuated beam to the energy distribution in the beam. The "threshold" for laser damage is derived from the energy density at the largest radius, Equation (1), at which a change in surface conditions can be detected in a damage area resulting from a full unattenuated beam exposure. The second method is similar to the analysis used to obtain basic beam parameters. If it is assumed that the material under investigation possesses a definite threshold value, then the radius r_i of the damage area produced by an exposure through transmission T_i should be determined by Equation (1), with the experimentally determined value $a = 0.0256$ cm. A plot of $\ln(T_i)$ versus $(r_i/a)^2$ should be a straight line with an intercept at $r = 0$ of $\ln(T_c)$, where $T_c W_0$ is the value of transmitted energy density producing no observable effect on the sample. Both methods were used on Cu-1 vol% SiC. Only the second method proved applicable to exposures on the silver sample since the incident laser beam produced a melted spot with no indication of beam interaction outside the spot, Figure 16.

RESULTS

Evaluation of Damage on Superpolished Cu-1 vol% SiC Specimen

A Nomarski photomicrograph of a damage area resulting from the unattenuated beam incident on the Cu-1 vol% SiC specimen 045 #39 is illustrated in Figure 14. The damage area at the resolution of the photo can be roughly divided into four damage levels. The first

indication of change in surface condition occurs at a radius of about 0.02 cm. This is indicated in Figure 14 as position 1. A slight darkening of the surface, indicating a slight change in surface topography, can be seen at that radius. A more pronounced change in surface texture can be seen at position 2 (~ 0.016 cm radius). This change strongly suggests enhanced interaction of the beam with scratches and blemishes. At position 3 (~ 0.011 cm radius), large scale distortion of the surface is observed. Finally, a molten metal region is observed at position 4 (~ 0.0023 cm radius). Energy densities corresponding to the radii at each of the positions as derived using the beam parameters given in Equation (2) are presented in Figure 14. The threshold for change in surface conditions can thus be taken to be approximately 136 joule/cm^2 , corresponding to the outermost detectable change in surface condition.

In two other full-beam exposures on Cu-1 vol% SiC (sample 045 #39), the inner structure of Figure 14 was not reproduced in detail, but the boundary associated with increased interaction with surface topography was reproducible. A central spot of increased damage and its characteristic radius was also evident in other full-beam exposures. The value of $136 \pm 10 \text{ joules/cm}^2$ is therefore judged to be a valid value of the threshold for the interaction between the wings of the Gaussian focal spot and the surface on this sample. If 136 joule/cm^2 however, is to be interpreted as the threshold for damage, then exposures with the beam passing through attenuators with transmission less than 0.54 to provide 136 joules/cm^2 , should produce no effect on the sample. This was not observed to be the case.

Results obtained by the second method of analysis of damage on Cu-1 vol% SiC 045 #39 sample are illustrated in Figure 15, a graph of $\ln(T_i)$ versus $(r_i/a)^2$. The radii used were the maximum at which surface effects could be observed for the beam attenuation T_i used in the corresponding exposure. The intercept at $r = 0$ yields a threshold attenuation value of $T_c = 0.139$. The energy density derived from this attenuation threshold is 35 joules/cm².

In summary then, the above data indicate that the two methods of evaluating damage threshold produce different results. This subject will be treated in the Discussion section.

Evaluation of Damage on Silver Coated Specimens

A Nomarski photograph of damage produced by a typical unattenuated exposure of the silver coated sample is illustrated in Figure 16. The most striking aspect of this damage is that, in contrast to the results on the Cu-1 vol% SiC specimen, no effects which can be unambiguously related to interaction with surface topography can be seen. The general appearance exhibited in Figure 16 was reproduced in all exposures on the silver coated sample. The attenuated beam produces melting, presumably in the center of the focal spot, with the radius of the molten region decreasing with increasing attenuation. Application of the second method of damage analysis as above for Cu-1 vol% SiC results in the curve illustrated in Figure 15. An attempt to apply the first method to the damage area resulting from the unattenuated beam produced inconsistent results. Extrapolation of the data in Figure 15 for the silver overlayer to $r = 0$ results in an attenuation $T_c = 0.175$ which corresponds to a damage threshold of 44 joules/cm². Exposures on the

silver sample were made at various positions along a diameter. Since no evidence of debonding was observed the silver overlayer was felt to be in excellent thermal contact with its substrate over the entire mirror surface.

Evaluation of Damage by Other Laboratories

In independent earlier evaluations conducted by the Naval Weapons Center and Hughes Research Laboratory at the HRL damage facility, threshold values of 140 joules/cm^2 and 60 joules/cm^2 were found for Cu-1 vol% SiC and silver overlayers, respectively.⁽⁶⁾ These values are consistent with the result for silver, and that for the first process in Cu-1 vol% SiC reported here. Samples used in that experiment had been subjected to much handling and a variety of other tests, including FECO* measurements of surface roughness. FECO measurements require the deposition of silver and contact with a reference flat. No detailed comparison of results and effects was made.

DISCUSSION

Damage Threshold on Cu-1 Vol% SiC Specimen

Speculation regarding the origin of the disparate threshold results obtained for the dispersion hardened copper sample is warranted. Because of the apparent enhanced interaction of the beam with surface blemishes evident at level 3 in Figure 14, it is likely that the dependence of threshold value on method of analysis is related to effects resulting from instantaneous intensity excursions due to mode-locking in the beam. Further, since intensity is proportional to E^2 , where E represents the electric field strength, it is not unreasonable to

*FECO: Fringes of Equal Chromatic Order.

suggest that field enhancement due to surface blemishes contributes to the interaction of the beam with the surface.

Support for this contention is found in an analysis by Bloembergen who presented an analysis of field enhancement in dielectrics and discussed its implications for laser damage in transparent materials.⁽⁷⁾ Bloembergen provides an expression relating the field E within an imperfection to that in the bulk E_0 as:

$$E = \frac{1}{1 + L \frac{1 - \epsilon}{\epsilon}} E_0, \quad (3)$$

where L is a factor appropriate to a particular geometry. In the limit, for metals where the dielectric constant becomes very large, the relation becomes

$$E = \frac{1}{1 - L} E_0. \quad (4)$$

For a sphere, $L = 1/3$ and for a cylinder, $L = 1/2$. Thus if it is assumed that a cylindrical groove approximates a scratch and small pits approximate spheres, fields within surface blemishes can be between 1.5 to 2 times that in the unblemished surface.

The above discussion suggests a mechanism for damage which is highly sensitive to the detailed time history of the pulse. The different threshold results obtained may be due to variations in degree of mode locking over the aperture of the laser cavity, but experiments to verify the existence of such a variation have not yet been conducted. In the absence of further experiments it is reasonable to suggest that the 136 joule/cm^2 threshold value is appropriate for a smooth pulse with an equivalent duration of 470 nsec. The threshold of 35 joules/cm^2

is probably appropriate for pulses of extremely high peak intensity, i.e., up to a factor of 10 above the average value of 5.3×10^8 watts/cm².

Nature of Damage on Silver Coated Specimens

The absence of field enhancement effects in scratches etc. in damage areas on the silver coating is believed to be primarily the result of its higher conductivity to reduce the magnitude of the fields within the skin depth of the coating. An additional effect of the higher conductivity is that the melted areas in silver were much smaller than those in Cu-1 vol% SiC for comparable incident intensities. This indicates that interaction of the silver coating with the beam outside of the melted area would not start until higher values of incident electric field are reached. In addition, the difference in metallurgical condition i.e., strain, between the polishing scratches in the Cu-1 vol% SiC surface and the reproductions of these in the silver coating may contribute to a difference in behavior to laser damage.

CONCLUSIONS

Postexposure methods for laser damage threshold evaluation were established. One was based on relating energy distribution in the unattenuated beam to the radius of the damage area produced. The other was based on extrapolating the relation between damage area radius and attenuated beam energy to zero radius. For the Cu-1 vol% SiC mirror the two methods produced different damage thresholds. It is felt that the true threshold lies between the 136 and 35 joules/cm² values obtained for the first and second methods, respectively. Only

the second method could be applied to the silver coating and it resulted in a damage threshold value of 44 joules/cm². Of interest were the threshold values of 140 and 60 joules/cm² obtained by the Hughes Research Laboratory for Cu-1 vol% SiC and silver, respectively.

The distorted appearance of scratches in the damage area on the Cu-1 vol% SiC specimen suggested that field enhancement effects were operative. If so, the characterization of surfaces by means of statistical parameters is of questionable value in the interpretation of laser damage results. The actual topography at the point of interaction would be most important.

EVALUATION OF dc SPUTTERED SILVER AS A

HIGH REFLECTIVITY OVERLAYER

The evaluation of 1500 Å thick copper and silver high reflectivity overlayers deposited by rf-diode sputtering was reported in Phase II of the program.⁽²⁾ The best reflectivity obtained, 99.18% with sputtered silver, was lower than the 99.5% reflectivity obtained from UHV evaporated silver layers on polished quartz. In an attempt to improve the reflectivity of sputtered silver it was decided to employ supported-plasma dc sputtering in a high integrity sputtering system.

EXPERIMENTAL PROCEDURE

The sputtering system and hardware arrangement were the same as used for deposition of Cu-1 vol% SiC in Phase I of the program.⁽¹⁾ The sputtering system consists of a small volume, water cooled stainless steel vacuum chamber of BNW design with the chamber components sealed with Viton O-rings, none of which are exposed to the generated plasma. The vacuum chamber was pumped with a standard 2400 μ /sec oil diffusion pump combined with a 140 μ /min mechanical pump, and trapped with a high conductivity, high efficiency LN₂ trap.

The target-substrate and other hardware arrangement is illustrated in Figure 17. The MARZ-GRADE silver plate used for the target was simply placed on top of the water cooled dc sputtering electrode. The 1.52 in. diameter superpolished Cu-1 vol% SiC substrate was mounted in the substrate holder as illustrated in Figure 17. The substrate temperature was measured with a thermocouple imbedded in the holder in close proximity to the mirror substrate. The sputtering gas was

reagent grade krypton. The system was initially pumped to a pressure of $\sim 10^{-7}$ torr before introduction of the sputtering gas. The sputtering gas pressure in the system was maintained using a Granville-Phillips pressure controller coupled with a Schultz-Phelps ionization vacuum gauge. Operated as a dynamic system the sputtering gas flow through the vacuum chamber was regulated by a controller operated needle valve and variable conductivity bypass line to the vacuum pumps; i.e., furnishing controlled throttling of the pumps.

Typical conditions were:

Target Substrate Spacing	2.5 cm
Krypton Gas Pressure	10^{-3} torr
Substrate Etch	1 min @ -100 V & 5 ma
Substrate Temperature	3 to 225°C
Substrate Potential	Floating (≈ -15 V)
Target Voltage	100 V
Target Current	1.7 amp
Deposition Rate	$\approx 0.3 \mu\text{m}/\text{min}$

Discharge Conditions:

Plasma Voltage	24 volts
Plasma Current	2 amps

RESULTS AND DISCUSSION

Data on the influence of deposition temperature on surface roughness and absorption of the 1500 \AA thick dc sputtered silver overlayers are presented in Table 8.

Table 8. Influence of Deposition Temperature on Surface Roughness and Absorption of Sputter Deposited Silver Overlayers

Sample	Approximate Deposition Temperature (°C)	Surface Roughness (Å rms)		Absorption, %
		Cu-T Vol% SiC Substrate	Silver Overlayer	
T-1	204 max	20	56	0.832 ± 0.003
T-2	217 max	15	70	0.855 ± 0.034
T-3	168	18	37	0.893 ± 0.014
T-4	200	17	37	0.845 ± 0.027
T-5	120	15	30	0.801 ± 0.063
T-6	33	19	19	0.833 ± 0.018
T-5*	-	-	25	0.966 ± 0.051
T-6*	-	-	29	1.011 ± 0.081

*After annealing for 2 hrs at 100°C.

Although decreasing deposition temperature yields deposited silver surfaces with roughnesses near those of the starting substrate, a corresponding decrease in absorption was not observed. The rougher surfaces obtained at elevated substrate temperatures show about the same absorption. A possible explanation is that the rougher surfaced deposits made at elevated temperature have larger crystallites and higher conductivity. This would compensate for the loss due to their greater surface roughness.

Concerning deposit-substrate bonding it is significant that the deposits could not be separated from the substrate by using Scotch Tape,

thermal shock or mechanical scraping. These results indicate superior bonding relative to UHV evaporated films, which normally would fail such tests.

Two of the samples, T-5 and T-6, were annealed at 100°C for two hours in vacuo in an attempt to increase grain size in the silver and thus reduce absorption. The absorption of both samples increased. The increase could either be due to diffusion of substrate material into the overlayer, or contamination of the overlayer surface by the annealing environment. Since the annealing furnace was not UHV, surface contamination was probable. It is important to note that no consistent increase in roughness due to the anneal was observed. The roughness for Sample T-5 decreased, while that for T-6 increased.

It is pertinent to note that the techniques used in this work for surface roughness and absorption measurement do not provide the complete characterization of optical properties required to separate the influence of deposition and material variables for absorption research. Although electrical conductivity data would be helpful, the nature of the anticipated interaction between the silver deposit and its substrate would make resultant data difficult, if not impossible, to interpret. It is felt that an independent method for determination of the complex refractive index of thin, highly conductive overlayers deposited on conductive substrates in the infrared region of the spectrum is needed. An ellipsometer operating in the range from 9 to 13 μm would be ideally suited to this task.

CONCLUSION

The possibility of an increase in reflectivity through the use of dc sputtering was not observed. The properties of the dc sputtered silver overlayer were comparable to those produced by rf sputtering.

DEPOSITION OF DISPERSION HARDENED ALLOY ON MOLYBDENUM, CU=2 Wt% Be, AND TZM^R ALLOY SUBSTRATES

Since all previous Cu-1 vol% SiC deposits had been made on OFHC copper substrates it was of interest to demonstrate the feasibility of obtaining the desired deposit properties on other potential mirror support materials, such as molybdenum, Cu=2 wt% Be, and TZM^R alloy.

EXPERIMENTAL PROCEDURE

The sputtering hardware used was the four-substrate arrangement used in the Phase II work.⁽²⁾ A Cu-1 vol% SiC target was used for all depositions. The molybdenum, Cu=2 wt% Be and TZM^R alloy substrates were metallographically polished and cleaned as described earlier.⁽²⁾ The deposition parameters were identical to those used in the Phase II work.⁽²⁾

RESULTS AND DISCUSSION

Deposits were made on two each of the molybdenum, Cu=2 wt% Be, and TZM^R substrates furnished by Michelson Laboratory. One of each pair of the deposit-substrate combination were returned to Michelson Laboratory for evaluation. The deposit thicknesses were 0.323 mm on molybdenum, 0.39 mm on Cu=2 wt% Be and 0.33 mm on TZM^R.

The remaining deposit-substrate combinations of each pair were retained for evaluation at BNW. Material was removed from the surface of each deposit by machining, leaving in each case a deposit thickness of 0.25 mm. The primary reason for material removal was to ensure parallelism between the deposit surface and the back surface of the substrate. Machining the deposit surface was also a good test of deposit adherence to the substrate. The specimens were polished using the BNW india ink technique described in earlier work. (1)

Based on the results presented in Table 9, no significant difference in polishability or optical absorption at 10.6 μm was noted for the deposits on the three substrate materials.

Table 9. Optical Characterization of Cu-1 Vol% SiC Deposit on Indicated Substrate Materials

<u>Substrate</u>	<u>Surface Roughness, Å, rms</u>	<u>Absorption, %</u>
Cu=2 wt% Be	15	1.74
Molybdenum	16	1.61
TZM ^R	13	1.78

The results obtained by Michelson Laboratory using a pitch lap polishing technique yielded surfaces of $\approx 16 \text{ \AA}$ rms roughness and flatness within $1/4 \lambda$ ($\lambda = 5461 \text{ \AA}$). (6)

CONCLUSION

It was found that the different substrates did not have any measurable effect on deposit polishability. The 16 \AA rms surface roughness obtained by Michelson Laboratory was essentially identical to the $13\text{-}16 \text{ \AA}$ rms range obtained by BNW.

EFFECT OF RECRYSTALLIZATION ON SURFACE FINISH

Since the Phase I work⁽¹⁾ had established that recrystallization would occur in the Cu-1 vol% SiC sputtered deposit at temperatures $\approx 350^{\circ}\text{C}$ it was decided to determine whether recrystallization would seriously degrade the surface finish. Accordingly, the deposit on mirror blank LM044-31 was superpolished to a surface roughness of 19 \AA rms. After a one-hour heat treatment at 450°C in vacuum to produce recrystallization, it was found that the surface roughness had increased to 50 \AA rms. The increase in surface roughness is illustrated in Figure 18, with Nomarski photographs of the surface before and after heat treatment. This result indicates, that depending on the application, additional work may be required to improve the thermal stability of the grain structure in the sputtered deposit.

CONSTRUCTION AND PRELIMINARY EVALUATION OF A DIFFERENTIAL CALORIMETER FOR MICHELSON LABORATORY

At the request of Michelson Laboratory, a portion of the contract effort was diverted to fabricating a duplicate of the calorimeter developed by BNW in the Phase I work for their use. A calorimeter is not as sensitive to flatness as the absolute reflectometer in the Michelson Laboratory, and hence reduces figure requirements for reliable absorption measurements.

Detailed calibration of the device was not performed, but enough was done to verify that it operated correctly. Measurements indicate a time constant near 11 minutes, an area sensitivity of about 3.8

millijoule per microvolt minute, and a deflection sensitivity of 0.046 joule per μ volt. The calorimeter actually possesses 14% higher area sensitivity and 30% greater deflection sensitivity than the one in use at Battelle-Northwest. The greater sensitivity is probably due to the fact that construction and assembly procedures were improved by our prior experience.

Unfortunately, the device was the victim of rough handling during its initial shipment. It was returned for repair by a Michelson Laboratory representative on the occasion of a routine program review. This event permitted detailed instruction of Michelson Laboratory personnel in its operation.

ACKNOWLEDGMENT

The author wishes to express his gratitude for the contributions made to this report by R. L. Gordon, B. P. Hildebrand, R. H. Beauchamp, H. G. Barrus, Nils Laegreid, and H. R. Gardner of the Battelle-Northwest Laboratories. Also to C. T. Walters of Battelle Columbus Laboratories, and to other members of both laboratories assisting in the performance of the work.

The financial support of DARPA is also acknowledged.

REFERENCES

1. R. W. Stewart, Investigate Material Systems for Mirrors Used in High Power CO and CO₂ Lasers, Semiannual Technical Report, BNWL-1780, Battelle-Northwest, Richland, WA, December 1972.
2. R. W. Stewart, Investigate Material Systems for Mirrors Used in High Power CO and CO₂ Lasers, Semiannual Technical Report, BNWL-1781, Battelle-Northwest, Richland, WA, August 1973.
3. E. Krekorian and R. J. Sneed, "Deposition Parameters Affecting Epitaxial Growth of Single Crystal Films," Transactions the Tenth National Vacuum Symposium, The MacMillan Co., New York, p. 368, 1963.
4. W. E. Spicer and T. M. Donovan, Journal of Noncrystalline Solids, 2: 66, 1970.
5. M. J. Braunstein, Hughes Research Laboratory, Malibu, CA, private communication, 1974.
6. M. J. Soileau and V. Wang, "Improved Damage Threshold for Metal Mirrors," Applied Optics, 13, 1286 (1974).
7. N. Bloembergen, Laser Damage--"Role of Cracks, Pores, and Absorbing Inclusions on Laser Induced Damage Threshold at Surfaces of Transparent Dielectrics," Applied Optics, 12, 661 (1973).

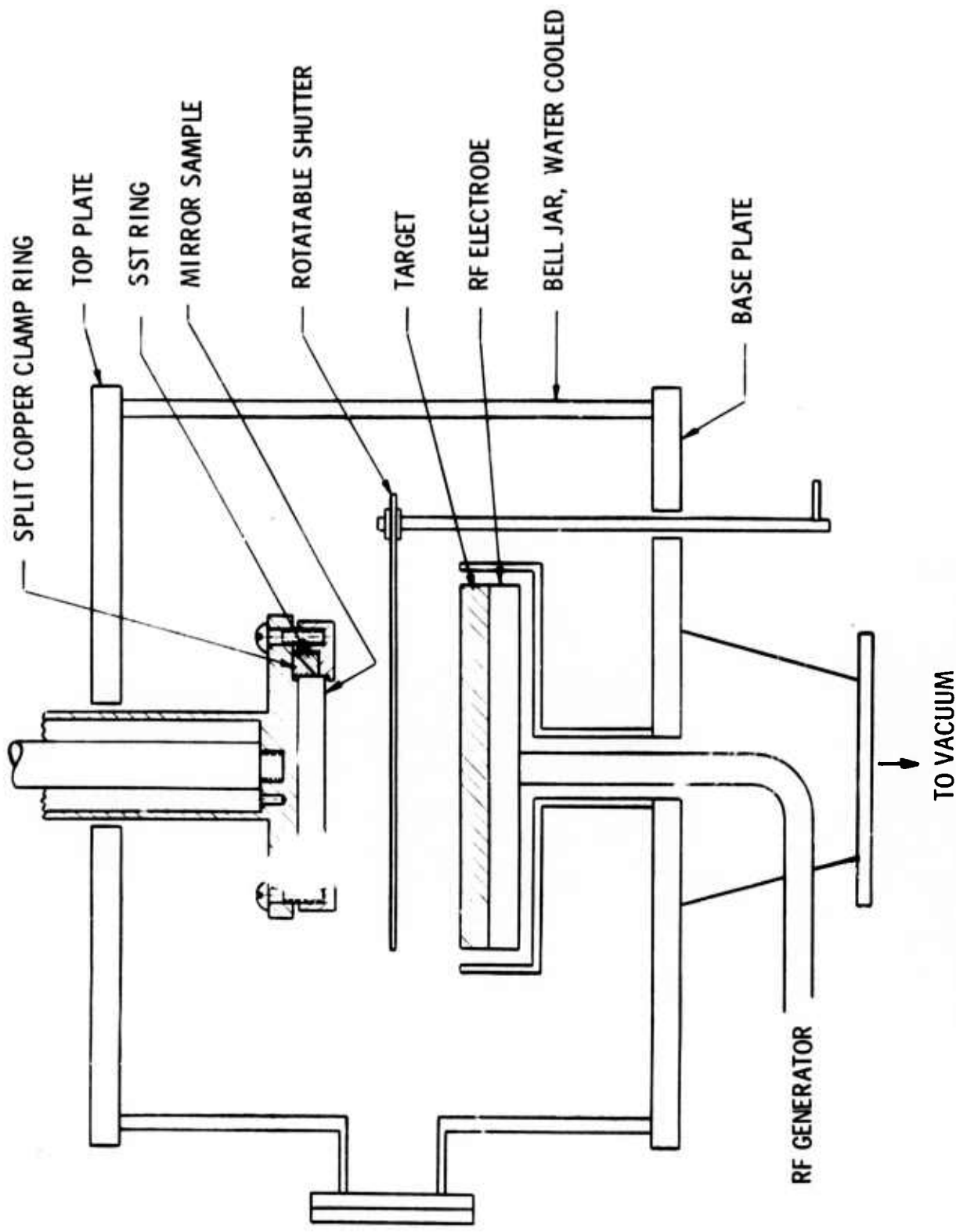


Figure 1. Electrode Arrangement for Deposition of Reflectivity Enhancement Coating Materials.

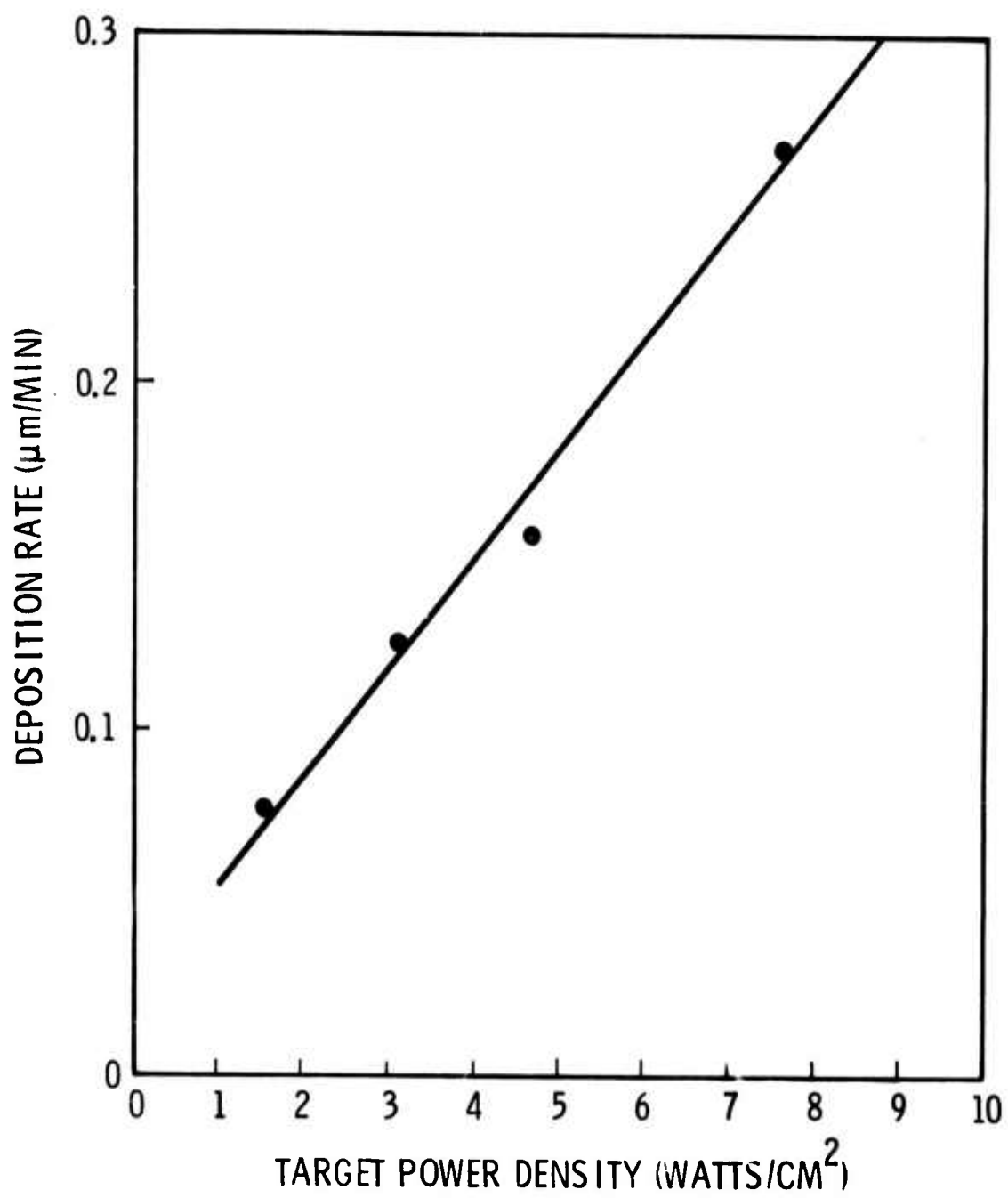


Figure 2. Observed Germanium Deposition Rate as a Function of rf Power Density at the Target

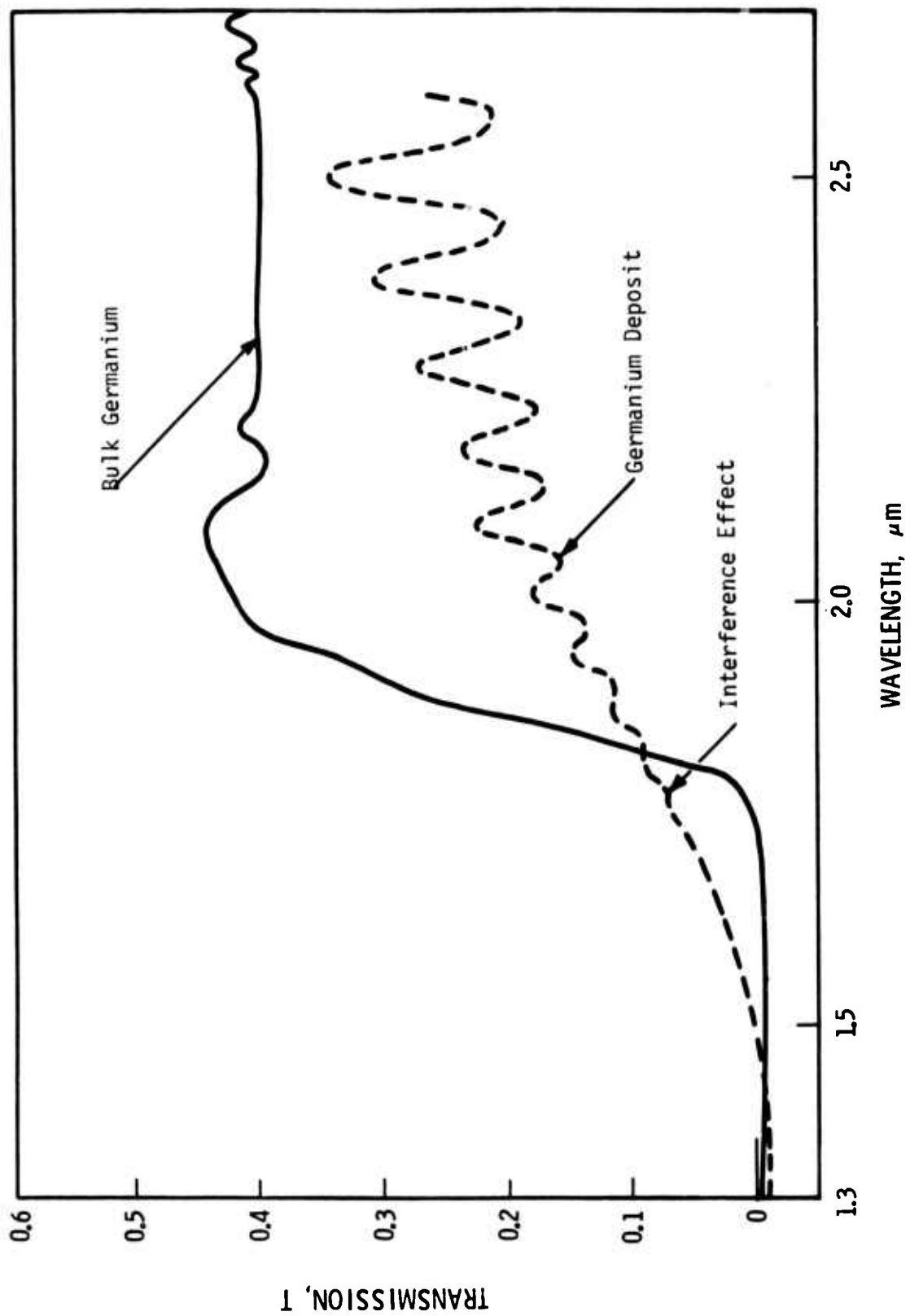


Figure 3. Transmission of Deposit Ge-NaCl #5 Near the Absorption Edge Compared to that for Typical Bulk Ge.

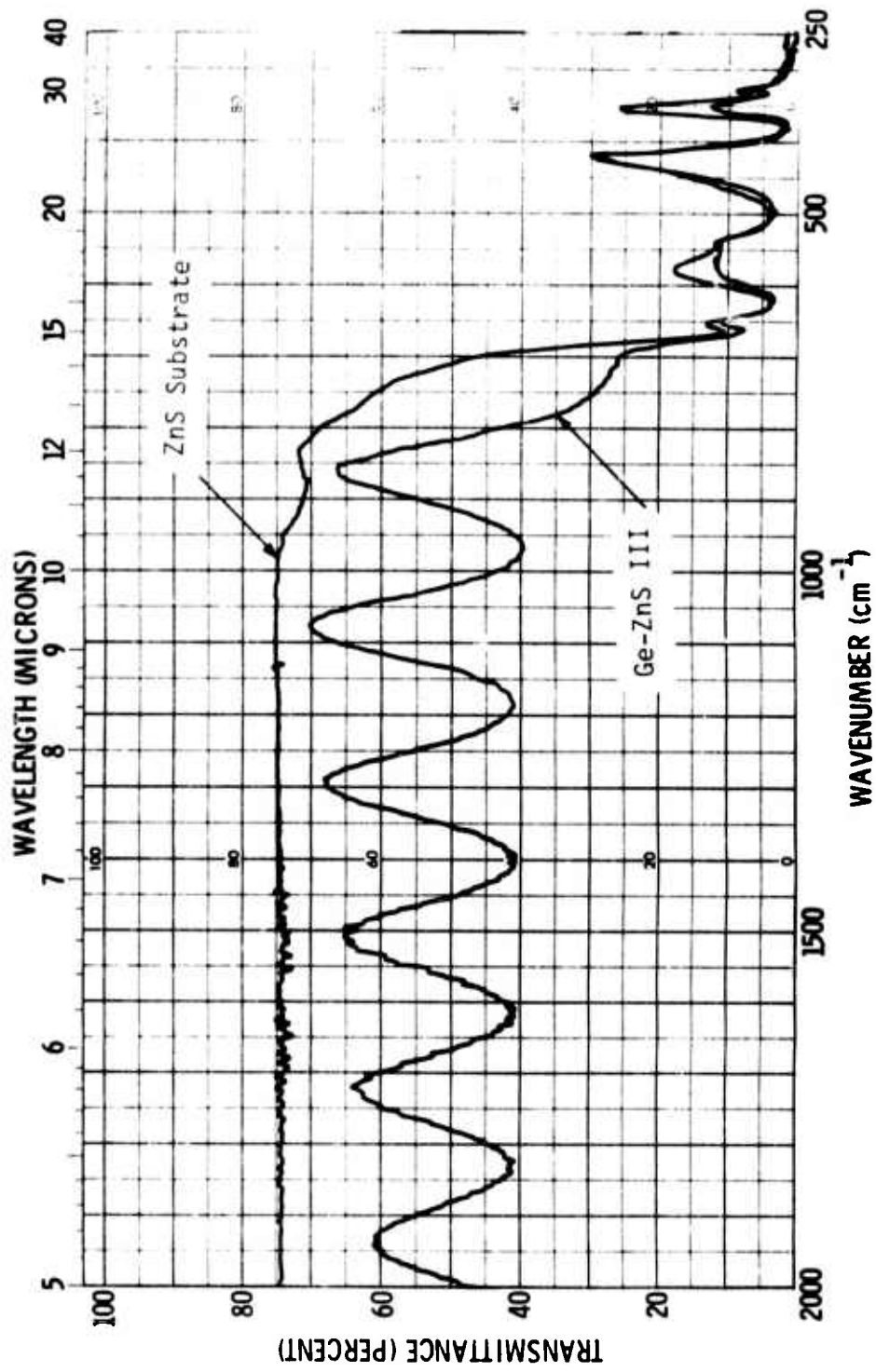


Figure 4. External Transmittance of Deposit Ge-ZnS III Compared to that of a Typical ZnS Substrate.

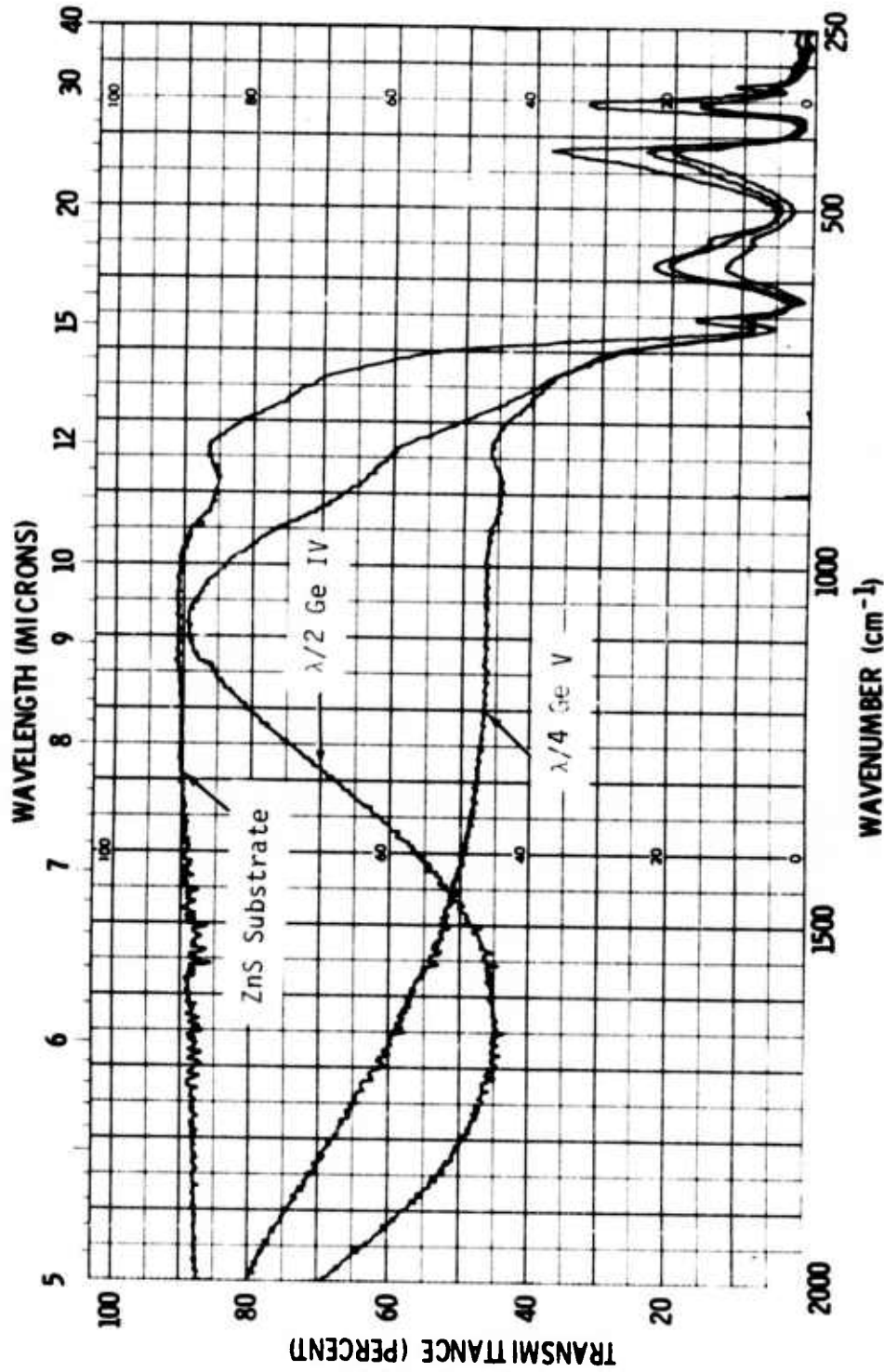


Figure 5. External Transmittance for Deposits-Ge-ZnS IV and V Compared to ZnS Substrate.

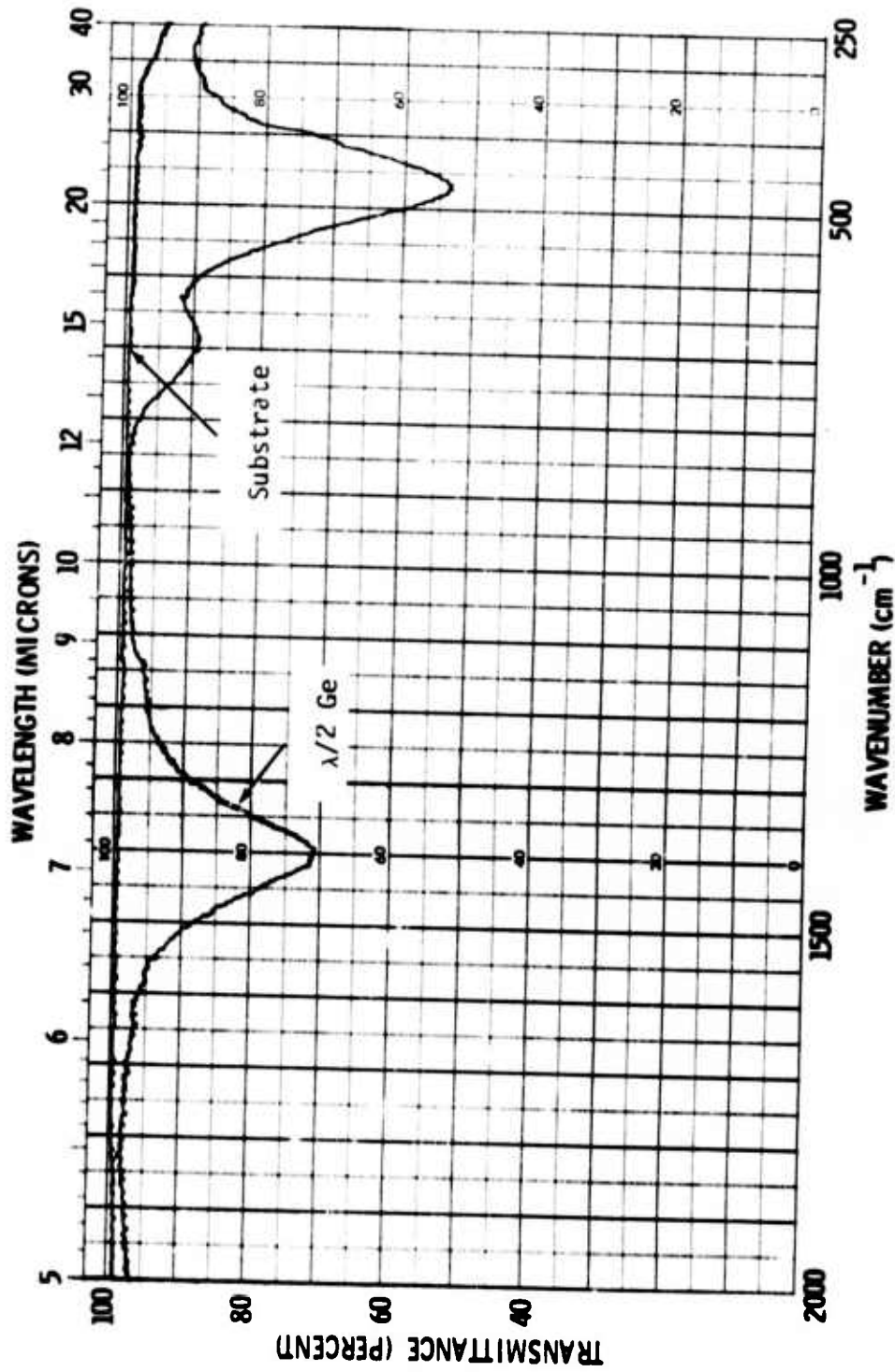


Figure 6. Reflection Spectrophotometric Results for a $\lambda/2$ Ge Deposit on BNW Mirror Substrate 044-#3. Optical Thickness is $1.016 \lambda/2$ at $\lambda = 10.6 \mu\text{m}$.

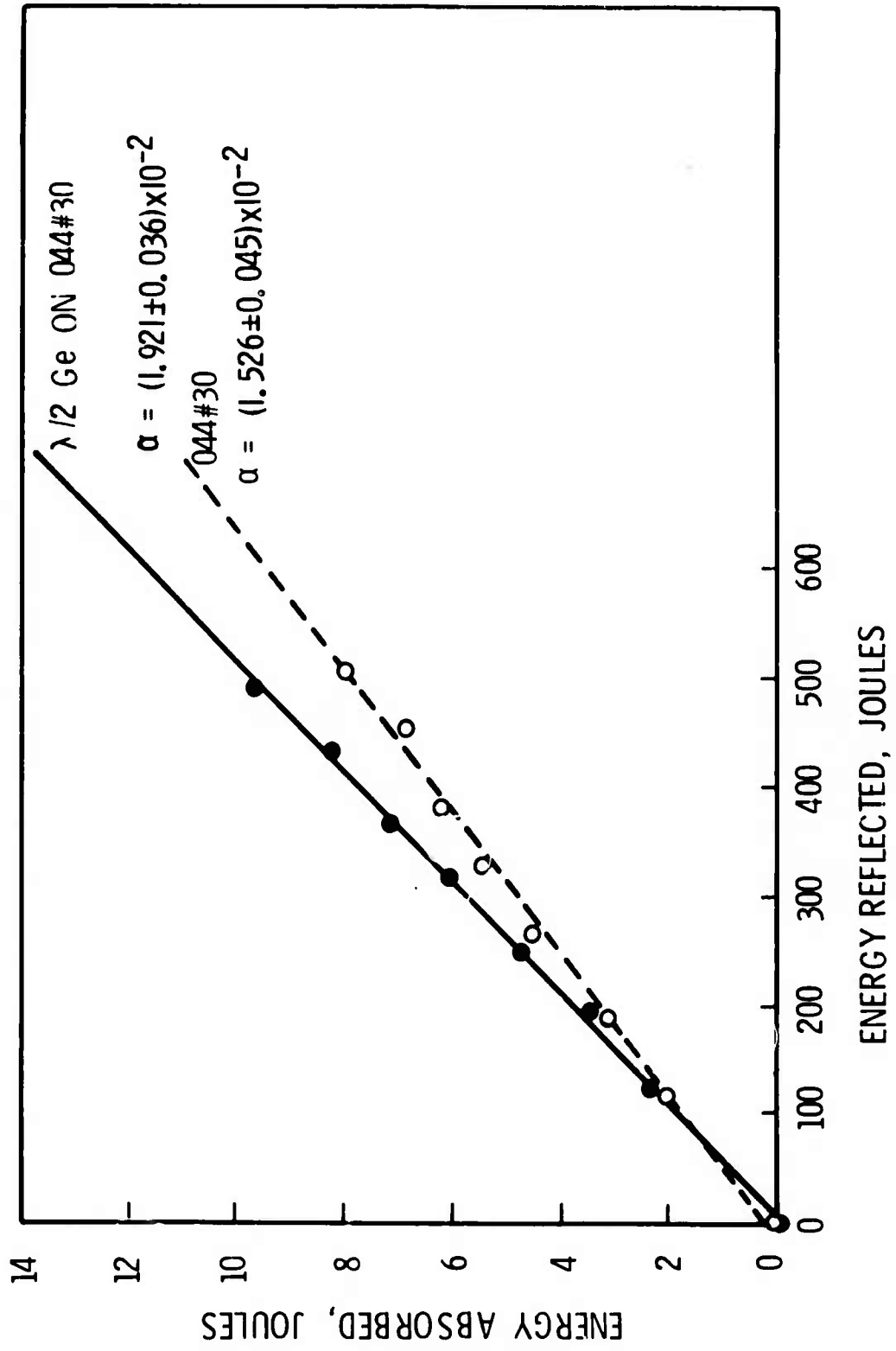


Figure 7. Absorption Data at 10.6 μ m Wavelength for BNW Mirror 044#30 Before (dashed line) and After (solid line) Deposition of a $\lambda/2$ Germanium Layer

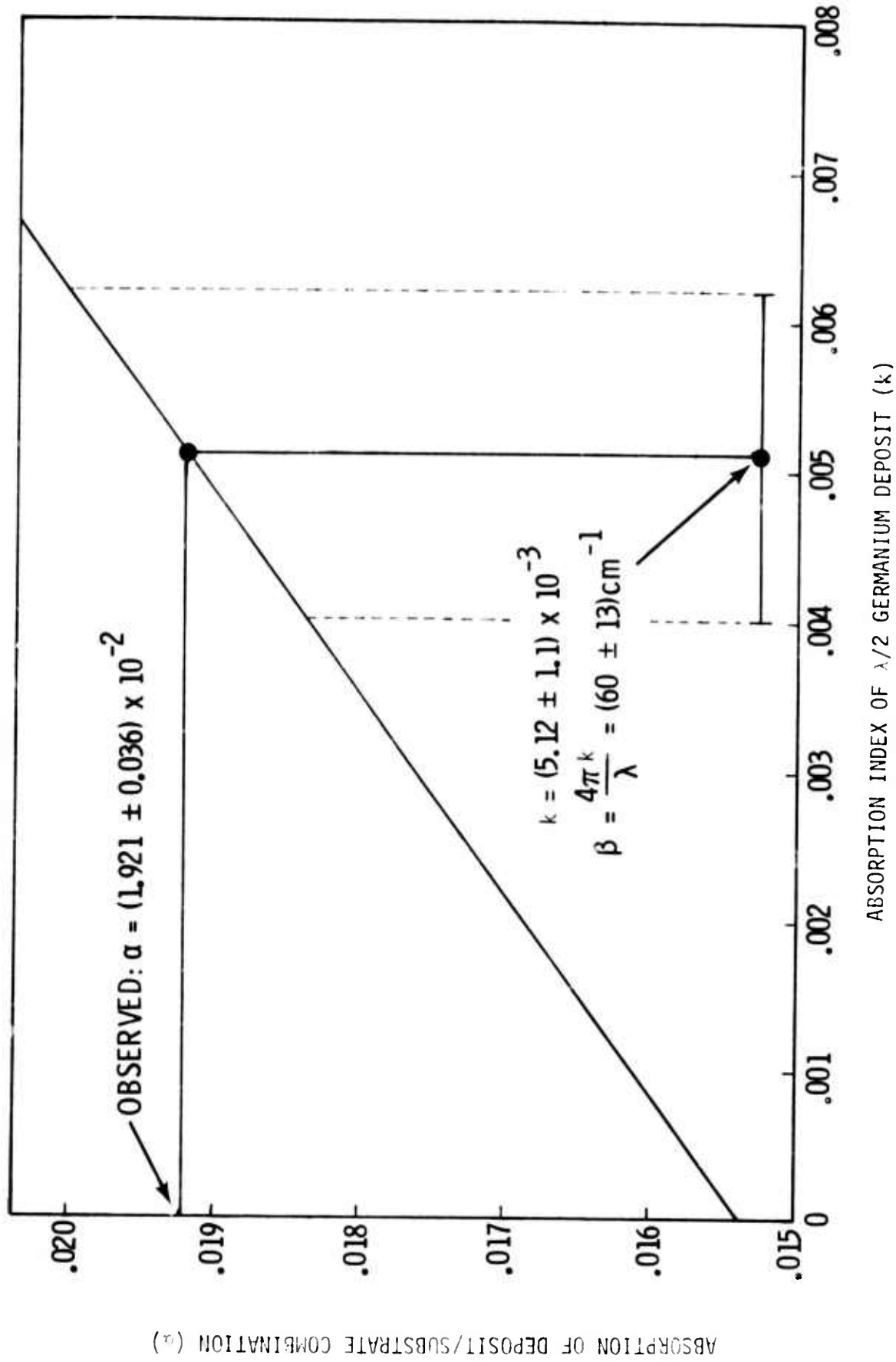


Figure 8. Relation Between Absorption Index of $\lambda/2$ Germanium Deposit and Absorption of Deposit/BNW 044#30 Mirror Substrate Combination. Values used in Establishing the Relation were $n = 4.07$, $k = 1.016 \lambda/2$. Error Bars Shown are Appropriate for the Observed Difference in Absorption

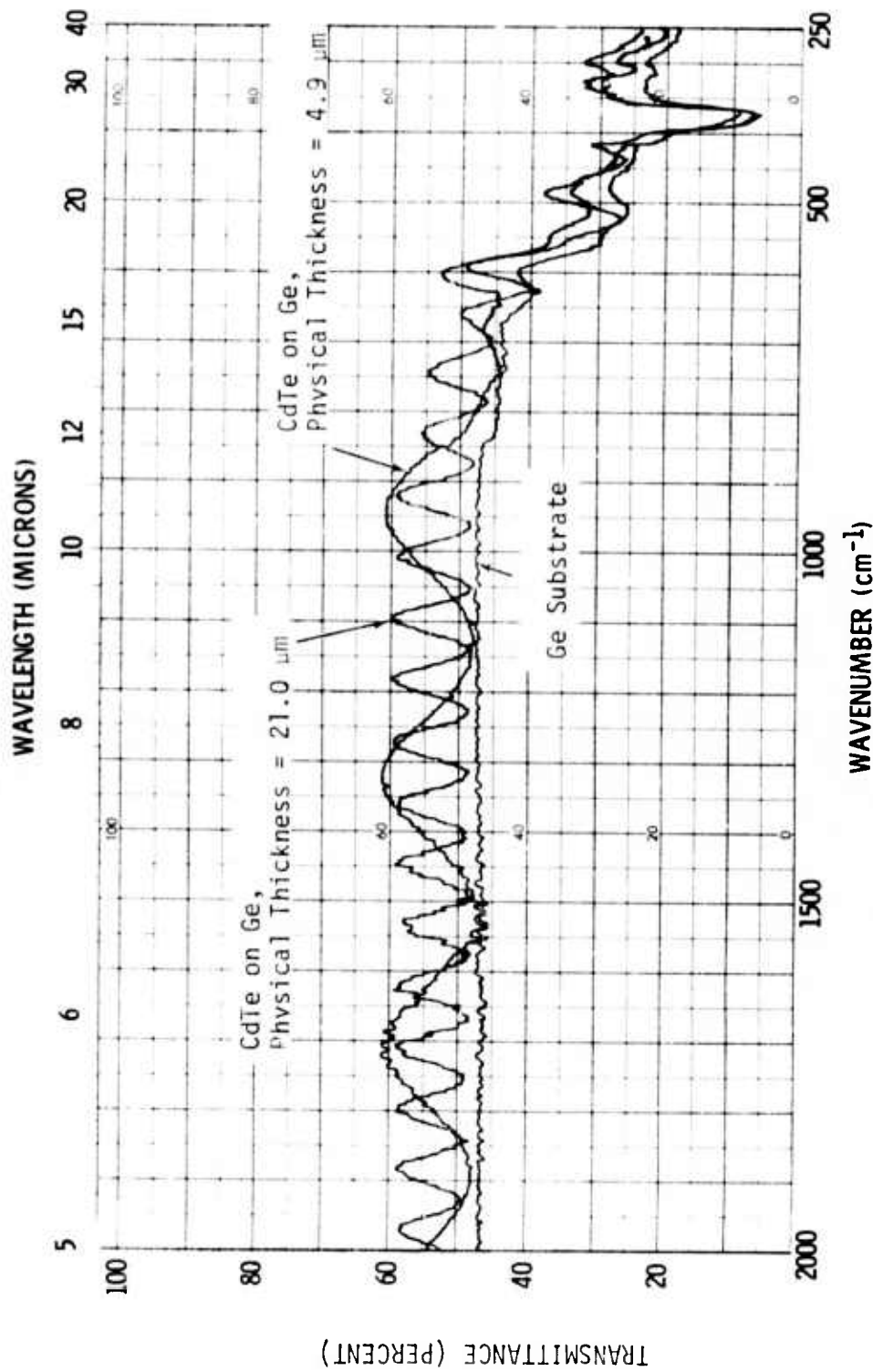


Figure 9. External Transmittance Obtained for Deposits of CdTe on Ge Substrates. Indicated Thicknesses are Estimates from Mass Increase and Deposit Area. Transmittance of a Typical Ge Substrate is Provided for Comparison.

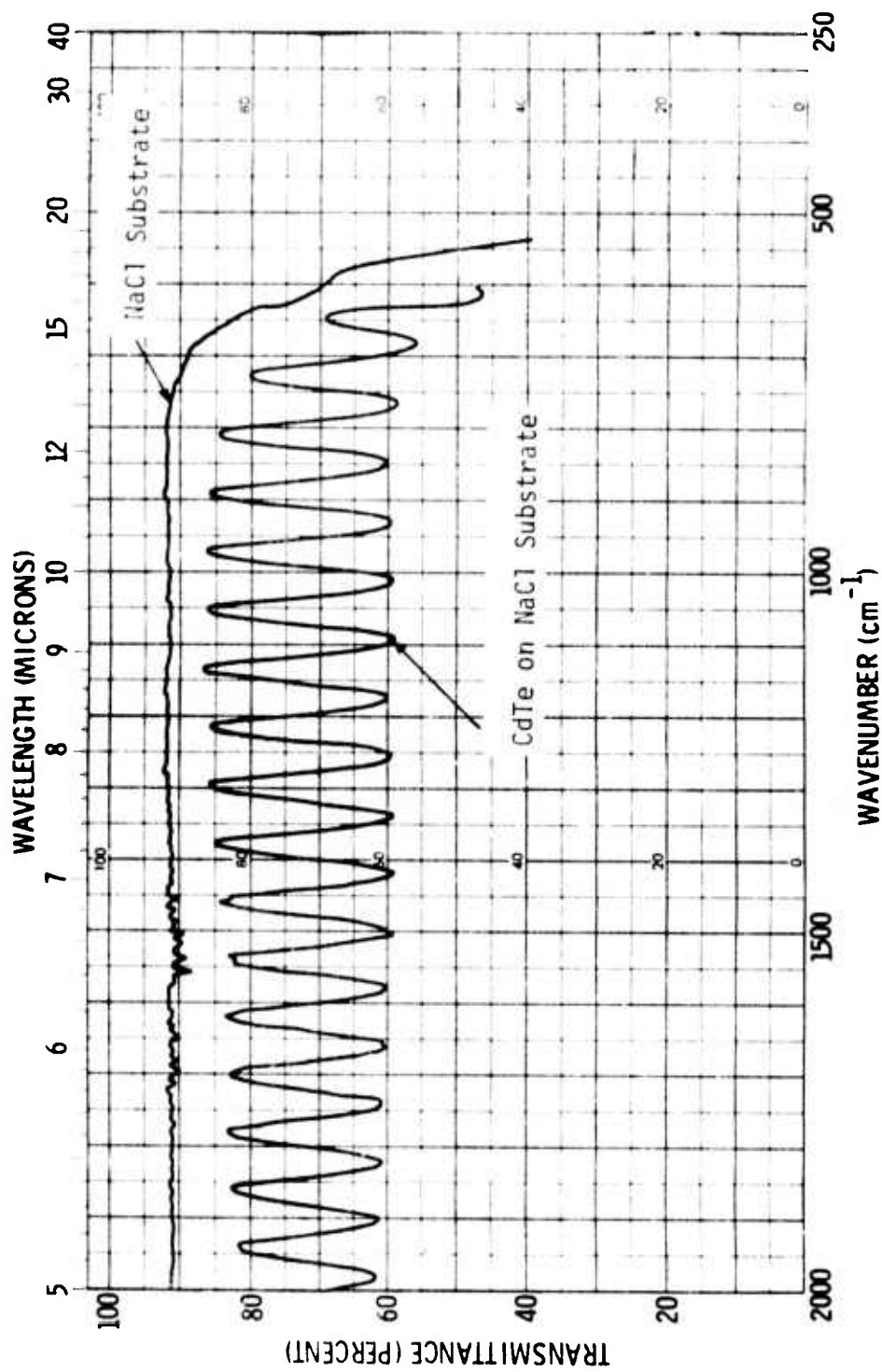


Figure 10. Transmittance Data Obtained from a 20.8 μm Thick CdTe Deposit on a NaCl Substrate Compared to the Transmittance of a Typical NaCl Substrate.

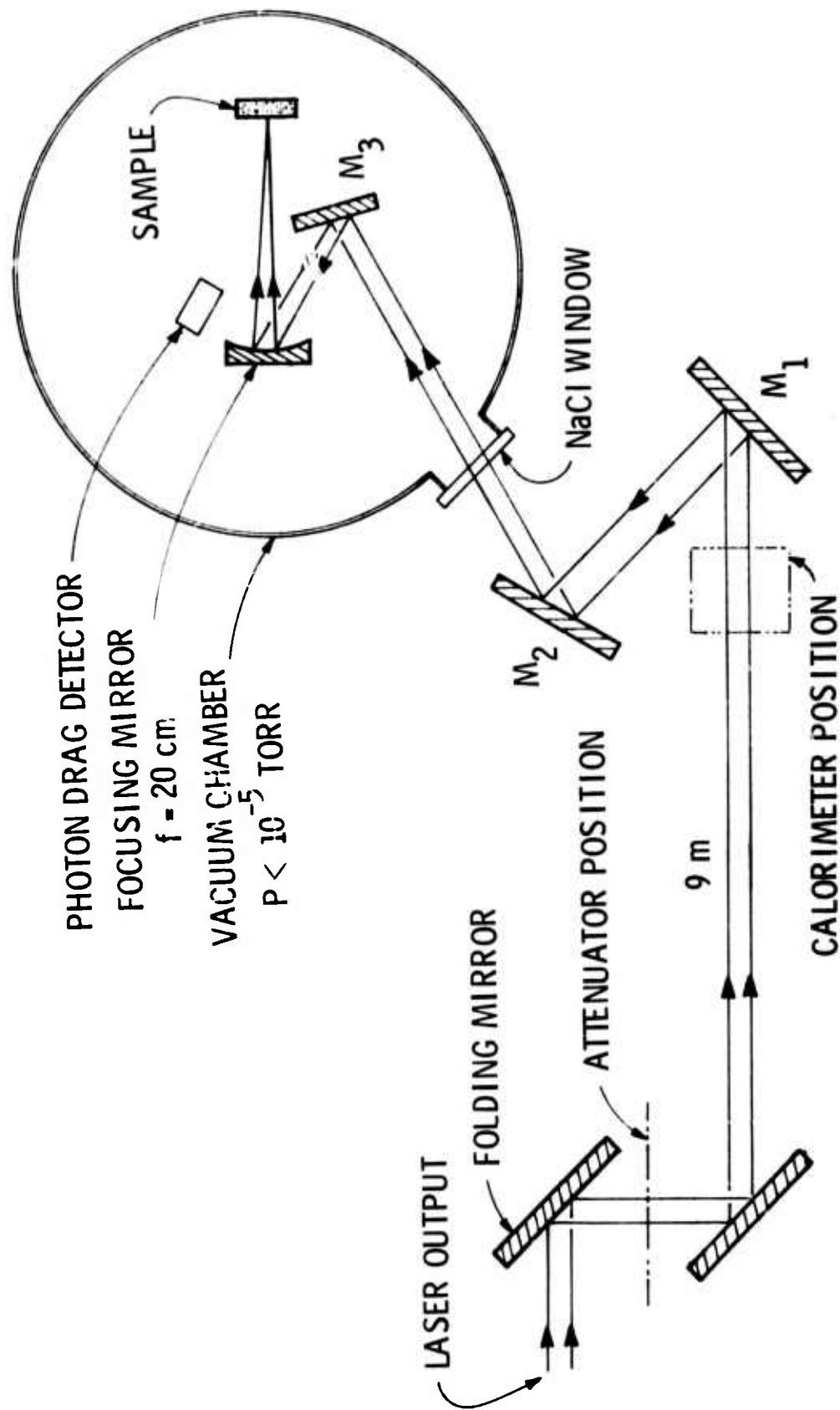


Figure 11. Arrangement of Optical Components, Vacuum System and Sample Position used in the Laser Damage Experiments

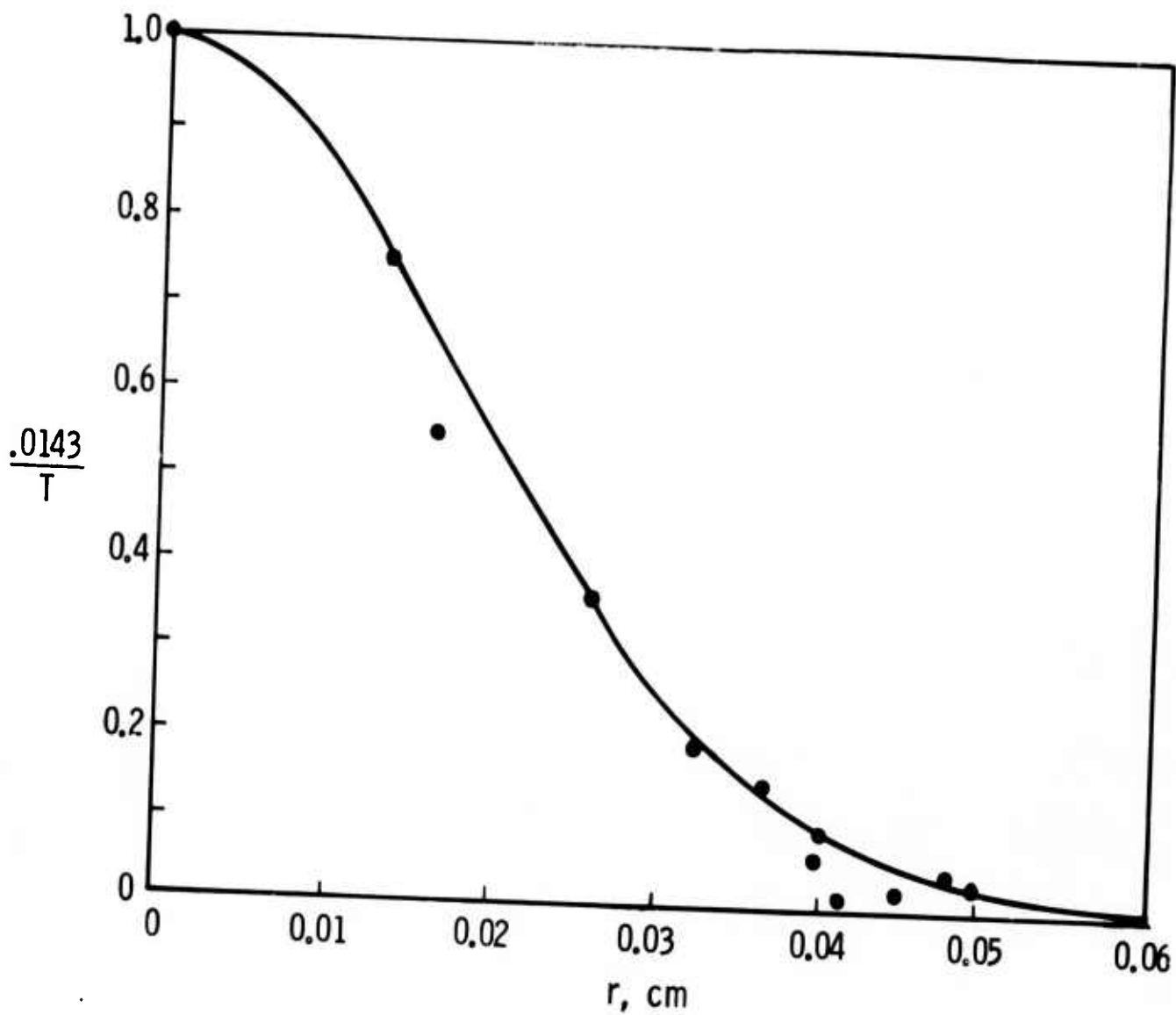
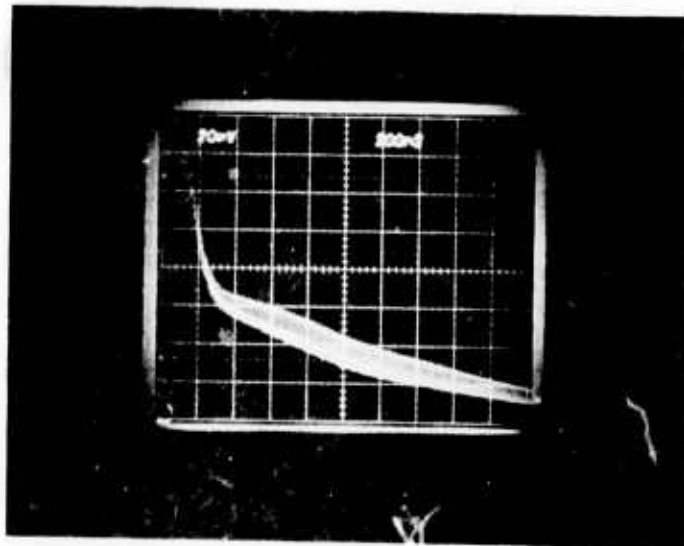


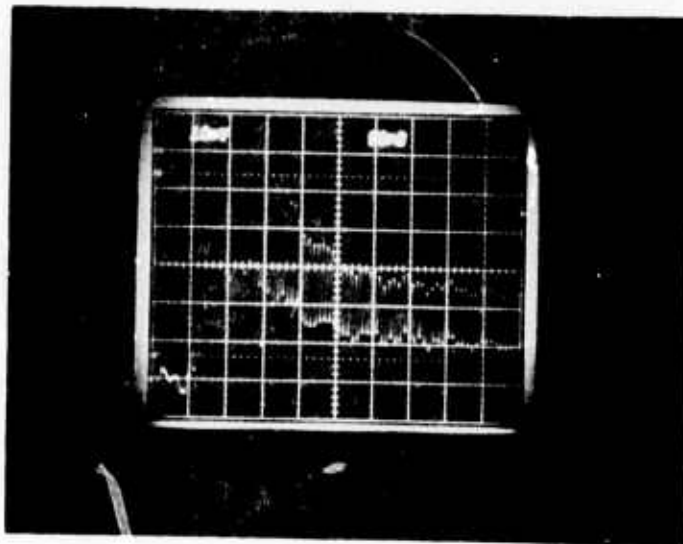
Figure 12. Gaussian Profile of Energy Distribution in the Focal Spot, Equation (1) with $T_c = 0.0143$. Filled Circles Represent Data Points with the Curve Resulting from a Least-Squares Fit to the Data

LASER POWER OUTPUT
(20 mV/Division)



TIME (200 nsec/Division)
(a)

LASER POWER OUTPUT
(10 mV/Division)



TIME (50 nsec/Division)
(b)

Figure 13. Time Dependence of Laser Power Output Determined with Photon Drag Detector, 180 mV/MW Sensitivity. Detector did not Intercept Entire Beam.

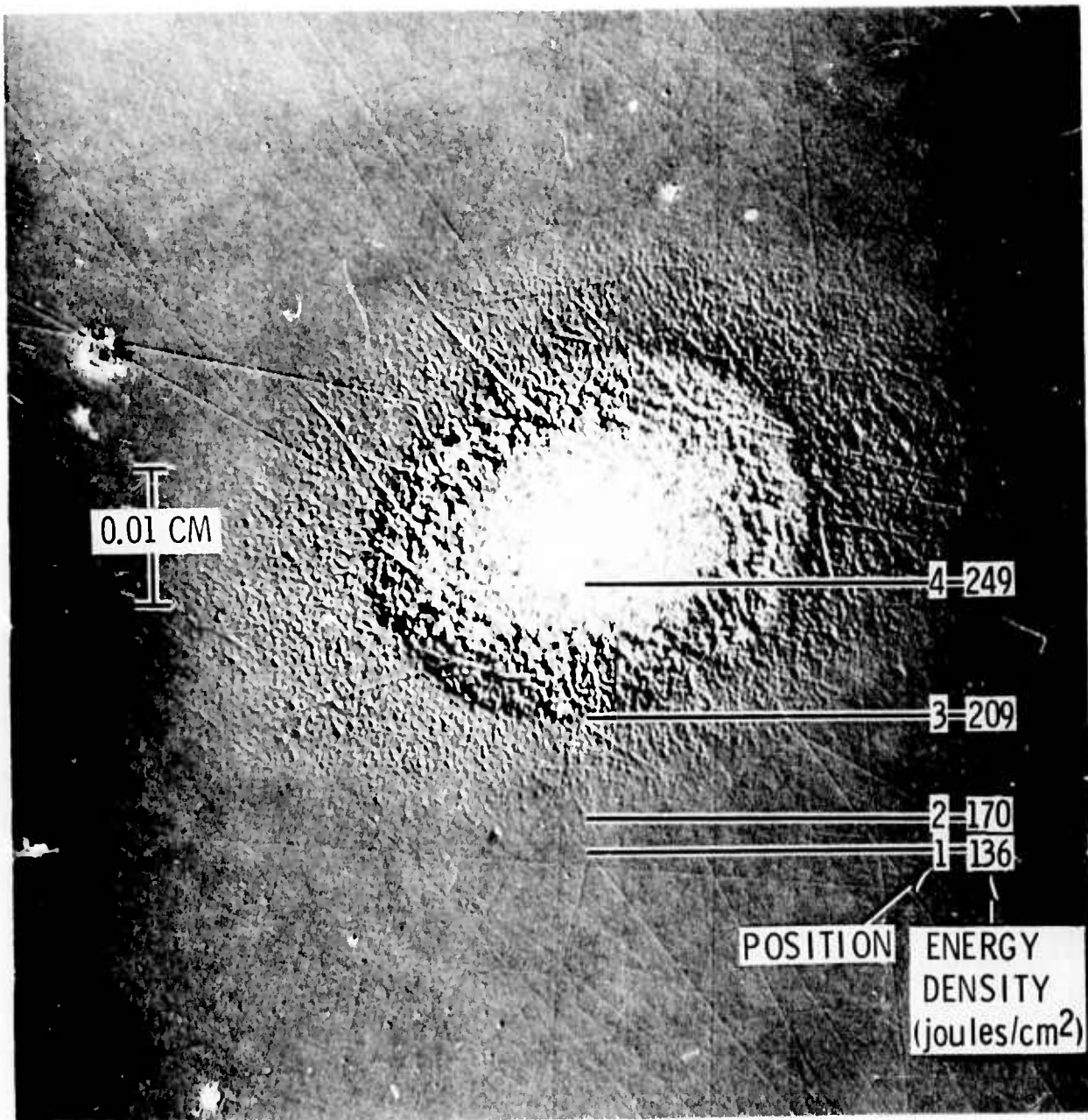


Figure 14. Damage Area on Cu-1 Vol% SiC Sample, Resulting from an Unattenuated Beam Exposure. Radii Identified by Numbered Lines Delineate Regions of Detectable Difference in Surface Interaction to the Beam. Nomarski Photograph.

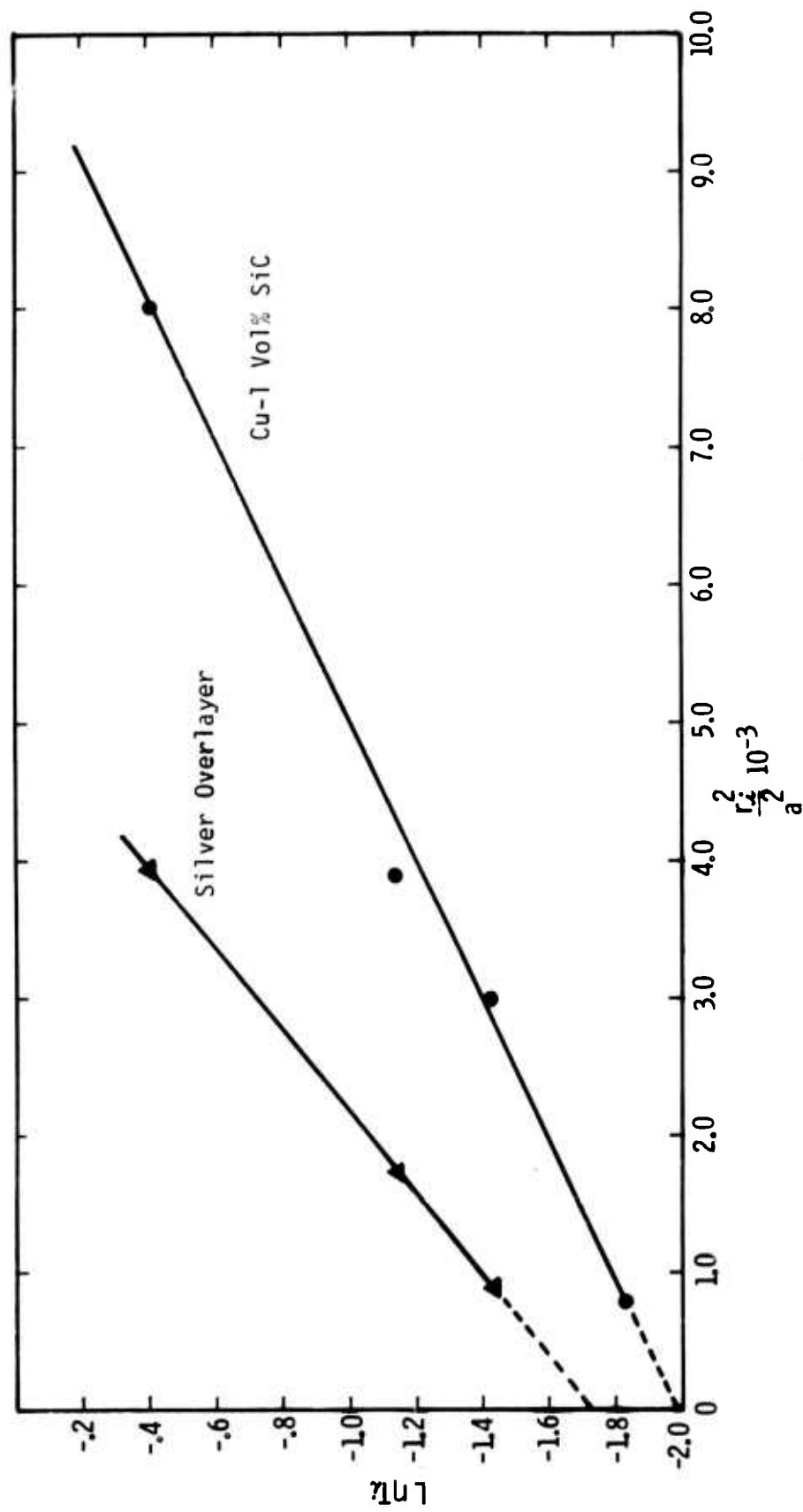


Figure 15. Damage Threshold Determination for the Silver Overlayer, and the Cu-1 Vol% SiC Specimen. Data Represent Actual Measured Damage Spot Radii at the Indicated Transmission, T. Damage Thresholds are Derived from the Curve Intercepts with the Ordinate at $r = 0$.

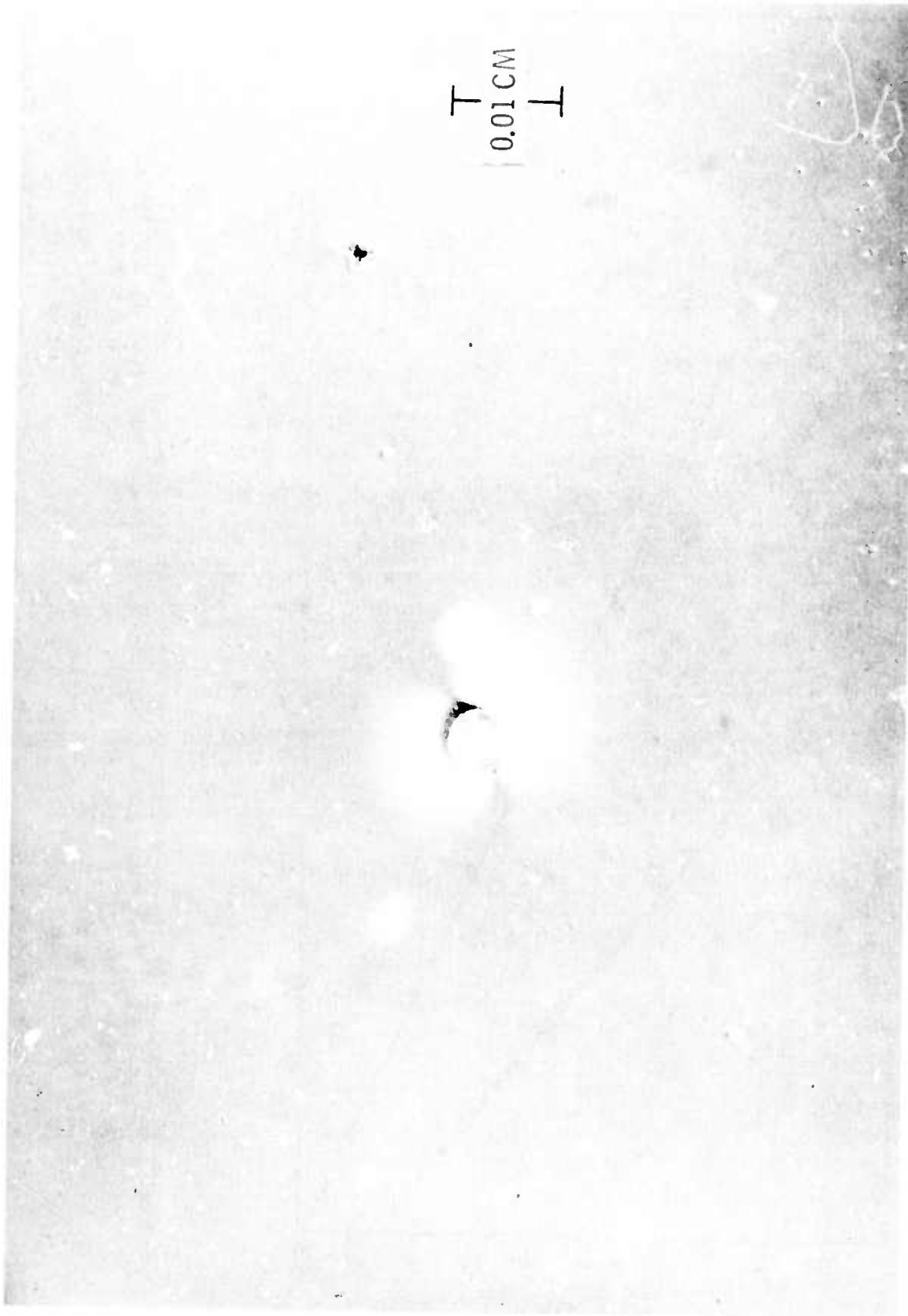


Figure 16. Damage Area Produced on the Silver Coated Sample by an Unattenuated Beam Exposure. Nomarski Photograph.

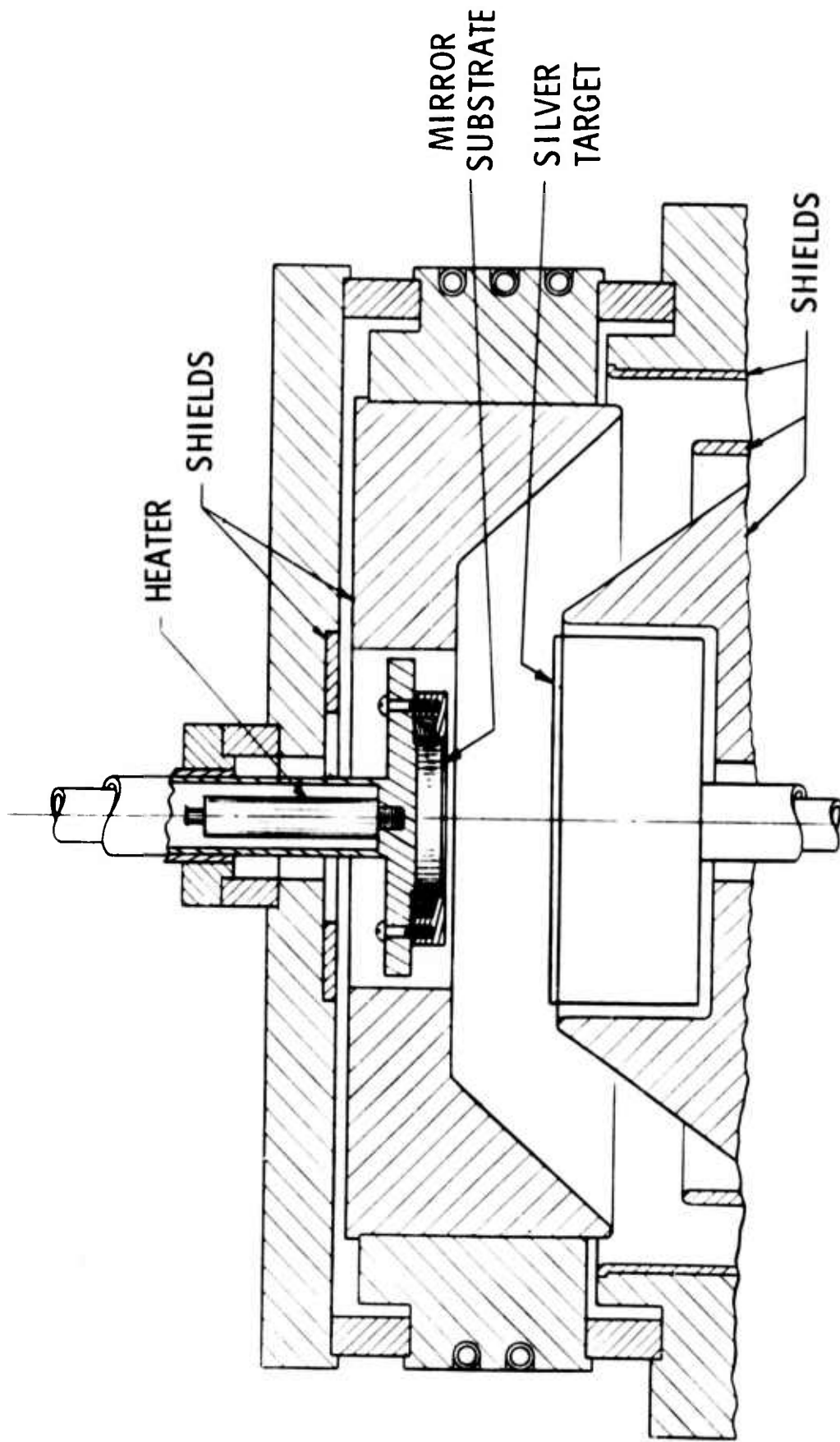
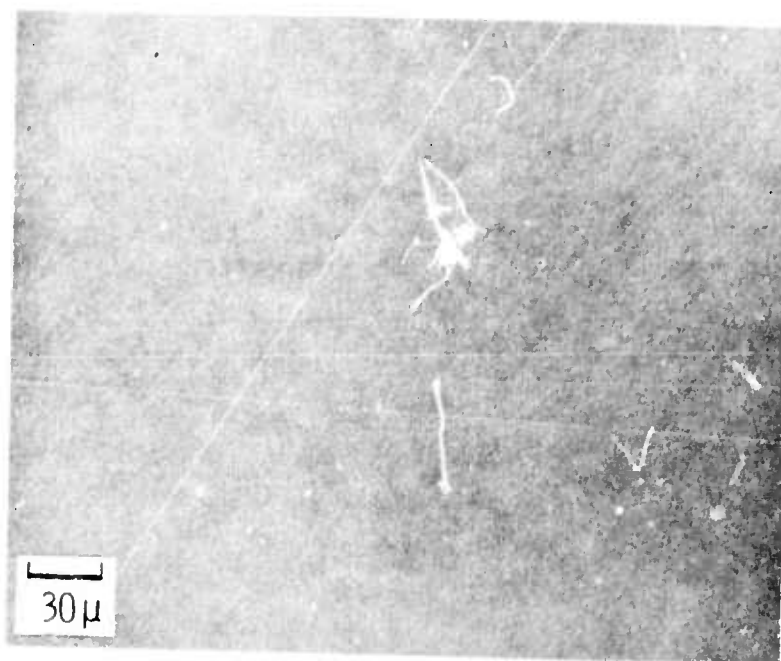
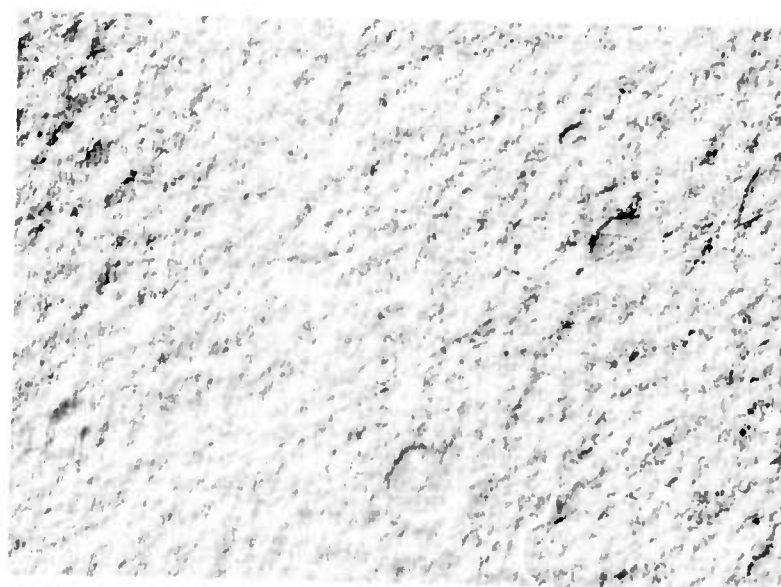


Figure 17. Electrode Arrangement for Deposition of Silver High Reflectivity Overlayers



Before Heat Treatment: 19 Å rms



After Heat Treatment: 50 Å rms

Figure 18. Influence of Recrystallization, Caused by in vacuo Heat Treatment for One Hour at 450°C, on Surface Roughness. Specimen LM044#31, Nomarski Photograph.

APPENDIX A

Theoretical and Experimental Considerations Important to Film Characterization

Complete characterization of an optical film requires determination of its complex index of refraction, $n + ik$. The imaginary part of the refractive index, or the absorption index, determines film absorption. The extinction coefficient of the material, β , is given by

$$\beta = \frac{4\pi k}{\lambda_0} \quad (1)$$

The extinction coefficient is the inverse of the propagation distance in which the intensity of a wave with vacuum wavelength λ_0 falls to $1/e$ of its incident value, and hence determines absorption properties of the material. Unfortunately, there exists no simple relationship between calorimetric absorption of a film and its complex index of refraction. Characterization must be accomplished by comparing observed absorption to that calculated on the basis of electromagnetic theory.

The theory of layered media predicts that the reflection coefficient, r , and the transmission coefficient, t , are determined by a 2×2 matrix, M , the elements of which are functions of the complex indices of the layers ^(A1)

$$\begin{pmatrix} 1 + r \\ p_0(1 - r) \end{pmatrix} = M \begin{pmatrix} t \\ p_n t \end{pmatrix} \quad (2)$$

where, for a single film,

$$M = \begin{pmatrix} \cos \gamma_j & -\frac{i}{p_j} \sin \gamma_j \\ -ip_j \sin \gamma_j & \cos \gamma_j \end{pmatrix} \quad (3)$$

In Eqs. (2) and (3), the quantities p_j are given by

$$p_j = (n_j + ik_j) \cos \theta_j \quad (4)$$

where θ_j is the angle of incidence on the j th layers. Subscripts $j = 0$ ($j = n$) refer to the incident medium (substrate). The quantities γ_j are given by

$$\gamma_j = \frac{2\pi}{\lambda_0} (n_j + ik_j) h_j \quad (5)$$

where λ_0 is the free space wavelength of the radiation and h_j is the thickness of the j th layer. For a stack of films the matrix M is given by

$$M = M_1 M_2 \cdots M_{n-1} \quad (6)$$

where each M_j has the form of Eq. (3).

An interesting special case occurs for a no-loss layer or half-wave optical thickness. Letting $k_j = 0$ and $n_j h_j = \lambda_0/2$ in Eq. (5) yields,

$$\gamma_j = \pi$$

and the matrix M , Eq. (3), reduces to the unit matrix. Consequently, a half-wave layer with no loss has no measurable effect on transmissivity or reflectivity.

The reflection and transmission coefficients are obtained by solving the linear system Eq. (2), and the reflectivity R and transmissivity T obtained in the usual manner;

$$R = |r|^2, \quad T = \frac{n_n |t|^2}{n_0} \quad (7)$$

while the absorption in the layered medium is given by

$$A = 1 - R - T \quad (8)$$

Calorimetric absorption measurements of layers on metal substrates yield values for the quantity

$$\alpha = A + T = 1 - R \quad (9)$$

Characterization of a single layer thus requires calculation of α as a function of k_1 for the system (layer plus substrate) and comparison of the observed and calculated absorption. The correct k_1 value is that which mathematically predicts observed α .

A computer program employing complex arithmetic and suitable for two layers has been prepared and used for this task.

Minimal requirements for satisfactory characterization of a single layer include determinations of:

- The optical and geometrical thickness of the layer.
- The real part of the refractive index of the layer, n_1 .
- The refractive index of the substrate, $n_2 + ik_2$.
- Absorption of the system, layer plus substrate.

The techniques employed for these determinations will be discussed below.

Both optical thickness and index measurements have been performed on a Perkin-Elmer model 521 grating infrared spectrophotometer. Optical thickness measurements are made in both reflection and transmission by noting the wavelengths at which minima occur, i.e.

$$\lambda_m = \frac{4nh}{2m+1}.$$

Index measurements are made on layers deposited on transmitting substrates. The spectrophotometer gives values for the external transmittance as a function of wavelength, $T(\lambda)$, which because of multiple internal reflections is less than the interface transmissivity, $T_2(\lambda)$. Analysis indicates

$$T_2(\lambda) = \frac{2T(\lambda)}{1 + T(\lambda)} = \frac{4n_2}{(n_2 + 1)^2} \quad (10)$$

from which one obtains

$$n_2 = \left(\frac{2}{T_2} - 1\right) + \sqrt{\left(\frac{2}{T_2} - 1\right)^2 - 1} \quad (11)$$

where the subscript 2 refers to the substrate. The transmissivity of the layer-substrate interface is related to the external transmittance of the combination by

$$T_{12} = \frac{1}{\left(1 + \frac{1}{T}\right) - \frac{1}{T_2}} \quad (12)$$

and, at quarter wave points, it can be shown that

$$n_1^2 = n_2 \left[\left(\frac{2}{T_{12}} - 1 \right) + \sqrt{\left(\frac{2}{T_{12}} - 1 \right)^2 - 1} \right] \quad (13)$$

System operation and data reduction were sufficiently accurate to allow determination of the index of ZnS and germanium substrates to within 0.27% and 0.15%, respectively, of accepted values.

No definitive experimental determination of the complex refractive index of dispersion hardened copper substrates has been made. Fortunately, calculations indicate that, for low loss layers, results are not too sensitive to exact values for n_2 and k_2 for metallic substrates. This is true as long as the ones chosen predict the correct reflectivity of the bare metal substrate, i.e. as long as

$$R = \frac{(n_2 - 1)^2 + k_2^2}{(n_2 + 1)^2 + k_2^2} \quad (14)$$

For a no-loss layer at half-wave optical thickness, the above statement is exactly true, while for no-loss quarter wave layers, differences of only 0.15% in calculated transmissivities were noted. For low loss layers, i.e. $(k_1/n_1) \approx 10^{-3}$, two sets of (n_2, k_2) which predict the same metal transmissivity to within six significant figures, predict transmissivities of the half-wave-coated substrate which are the same to within five significant figures.

Other researchers rely on handbook values for n_2 and k_2 , but this approach would not be applicable to dispersion-hardened copper. We have used measured values of electrical conductivity and absorption at 10.6 μm in the Drude theory to estimate n and k for this work. The analysis is straightforward and results in the following equations for n and k :

$$n = \frac{1}{2} \left(\frac{2}{\alpha} - 1 \right) + \frac{1}{2} \sqrt{\left(\frac{2}{\alpha} - 1 \right)^2 - 2(1 + A^2)} \quad (15)$$

$$k = \sqrt{n^2 + A^2} \quad (16)$$

where α is the measured absorption of the sample and A^2 is related to radiation frequency ω , conductivity σ_0 , and relaxation time τ by

$$A^2 = \frac{4\pi\sigma_0\tau}{2\omega\tau + 1} - 1 \quad (17)$$

Parameters used in Eq. (17) were determined in Phase I. The average dc conductivity observed for Cu-1 vol% SiC deposits was $\sigma_0 \approx 1.585 \times 10^{17} \text{ sec}^{-1}$, while choice of $\tau \approx 8.2 \times 10^{-15} \text{ sec}$ produced a good fit of absorption vs. electrical resistivity data.

As previously reported, mirror absorption values are determined calorimetrically. Absorbed energy, E_a is determined by planimeter integration of the recorded calorimeter trace and reflected energy, E_r , by integration of the reflected power vs. time record produced by a CRL model 201 power meter. Mirror absorption, α , is then determined by,

$$\alpha = \frac{E_a}{E_a + E_r} \quad (18)$$

Absorption values presented earlier in this and in previous reports have been obtained by making three independent observations near the same E_r and quoting the average of these as the absorption. This technique was deemed unsuitable for determining the small absorption increase due to a $\lambda/2$ layer. The chosen method uses the linear relationship between absorbed and reflected energy implied by Eq. (18), i.e.,

$$E_a = SE_r; \quad S = \frac{\alpha}{1-\alpha} \quad (19)$$

Thus a plot of F_a vs. E_r should be a straight line with slope S and zero intercept. The absorption is determined from the slope of the line by

$$\alpha = \frac{S}{1+S} \quad (20)$$

A measurement is accomplished by making at least six successive exposures at ever-increasing values of E_r and the absorption and its standard deviation are derived from a computerized least squares fit to Eq. (19). Statistics of the fit obtained also provide valuable information regarding the operation of the instrument.

The calorimeter was recalibrated in a manner similar to that required for obtaining data with this technique. Electrical energies between 1.8 and 8.1 joules were deposited in the calibration sample via its internal resistor. A plot of area swept out on the calorimeter record vs. energy deposited in the sample was then made and a least squares fit performed. Results are shown in Figure (A-1). The calorimeter is linear over the entire range investigated. The correlation coefficient of the fit was 0.9989, compared to 1.0 for a perfect straight line. The slope of the line gives the calibration constant ($4.598 \pm .081$) millijoules per microvolt minute. It is interesting to note that calibration determinations throughout the course of the program have remained well within the $\pm 6.5\%$ absolute accuracy claimed for the calorimeter.

The weakest point in our absorption measurement has always been the measurement of reflected energy on the CRL power meter. Although satisfactory performance has been verified by comparison to a meter calibratable by substitutional power in the range below 3 watts, its performance in the operating range above 12 watts has not been checked. Recent work at Hughes Research Laboratories reported by Braunstein, ^(A2) indicates their meter was in error by 26.8%. This could also be the case with our instrument. An early check on the power meter calibration is planned.

The geometrical configuration of our experiment was originally determined on the basis of maintaining near-normal incidence. For this reason the power meter was placed 128.3 cm from the calorimeter, which permitted an angle of incidence

of only 3.47° . The sensitive area on the power meter is only 19 mm in diameter. Consequently, light scattered into angles greater than 7.5×10^{-3} radian from the specular direction could not be detected by the power meter. Although mirror surfaces generated under this program consistently exhibit roughness less than 20 Å rms, scatter due to the periodic nature of the surfaces, discussed in the Phase II Report, ^(A3) could conceivably affect the absorption results. Analysis indicates that, if α represents the ratio of absorbed to incident energy, then

$$\frac{\alpha'}{\alpha} = 1 - S \quad (21)$$

where α is given by Eq. (18) and S is the ratio of scattered to incident energy. Consequently, the true absorption is less than the indicated absorption. The error δ in absorption is related to the scattering coefficient S by

$$\delta = \frac{S}{1 - S} \quad (22)$$

To first order, then, $\delta \approx S$. Thus, a 1% error in absorption would result if 1% of the incident energy is scattered into angles greater than 7.5×10^{-3} radian. Scattering from the random background is well below the 1% level. Diffraction due to periodic structure on the surface is another matter. Although spacial wavelengths of the structure of $8.7 \mu\text{m} \leq \lambda \leq 12 \mu\text{m}$ were determined in Phase II of the program, ^(A3) no consistent effort to determine amplitude on the surface has been made. Consequently, an estimate of the scattering coefficient at $10.6 \mu\text{m}$ has not been made. For the purposes of this report we will merely state that values quoted for the absorption are to be considered upper limits. Any other statement without detailed calculations or measurements of total scattering from the periodic structure would be speculation.

One consequence of the small acceptance angle is extreme sensitivity to alignment. This has been known all along and proper alignment has always been rigorously adhered to throughout the course of the program. In the future, the calorimeter

will be placed closer to both the laser source and the power meter. Although some sacrifice in approaching normal incidence will be made, this will minimize effects of scattering on calorimeter absorption measurements by increasing the acceptance angle of the reflected power monitor. The use of a calibratable, reflecting power meter to monitor the incident beam, in addition to monitoring the reflected beam, would improve the measurement significantly.

References

- A1. Born, M; and Wolfe, E, Principles of Optics, Pergamon Press, Oxford, 1965, pp 51-70 and pp 627-633.
- A2. Braunsten, M; AFWL-TR-74-10, Low Absorption Coating Technology Final Report for period May 22, 1972 through May 22, 1973. March 1974.
- A3. R.W. Stewart, Investigate Material Systems for Mirrors Used in High Power CO and CO₂ Lasers, BNWL-1781, Battelle-Northwest, Richland, WA, August 1973.

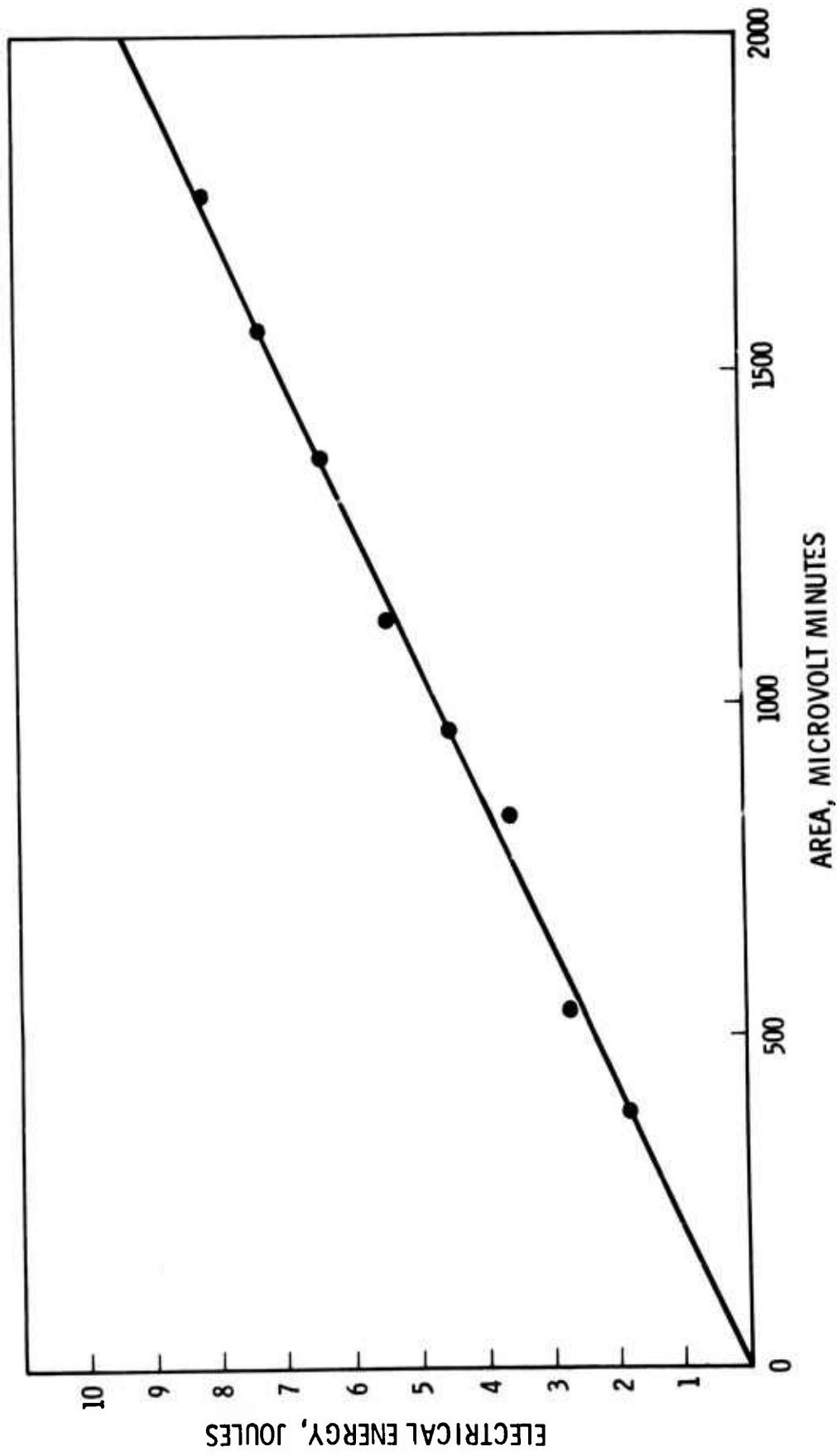


FIGURE A1. CALIBRATION DATA FOR THE CALORIMETER. FILLED CIRCLES REPRESENT DATA. THE LINE IS FROM THE LEAST-SQUARES FIT.